NEURODEGENERATIVE DISEASE

Antisense oligonucleotide–mediated MSH3 suppression reduces somatic CAG repeat expansion in Huntington's disease iPSC–derived striatal neurons

Emma L. Bunting[1]†, Jasmine Donaldson[1]†, Sarah A. Cumming[2], Jessica Olive[1], Elizabeth Broom[1], Mihai Miclăuș[3,4], Joseph Hamilton[1], Matthew Tegtmeyer[5], Hien T. Zhao[6], Jonathan Brenton[3,7], Won-Seok Lee[5,8], Robert E. Handsaker[5,8], Susan Li[6], Brittany Ford[6], Mina Ryten[3,7], Steven A. McCarroll[5,8], Holly B. Kordasiewicz[6], Darren G. Monckton[2], Gabriel Balmus[3,4], Michael Flower[1], Sarah J. Tabrizi[1]*

Expanded CAG alleles in the huntingtin (*HTT*) gene that cause the neurodegenerative disorder Huntington's disease (HD) are genetically unstable and continue to expand somatically throughout life, driving HD onset and progression. MSH3, a DNA mismatch repair protein, modifies HD onset and progression by driving this somatic CAG repeat expansion process. *MSH3* is relatively tolerant of loss-of-function variation in humans, making it a potential therapeutic target. Here, we show that an *MSH3*-targeting antisense oligonucleotide (ASO) effectively engaged with its RNA target in induced pluripotent stem cell (iPSC)–derived striatal neurons obtained from a patient with HD carrying *125 HTT* CAG repeats (the 125 CAG iPSC line). ASO treatment led to a dose-dependent reduction of MSH3 and subsequent stalling of CAG repeat expansion in these striatal neurons. Bulk RNA sequencing revealed a safe profile for *MSH3* reduction, even when reduced by >95%. Maximal knockdown of MSH3 also effectively slowed CAG repeat expansion in striatal neurons with an otherwise accelerated expansion rate, derived from the 125 CAG iPSC line where *FAN1* was knocked out by CRISPR-Cas9 editing. Last, we created a knock-in mouse model expressing the human *MSH3* gene and demonstrated effective in vivo reduction in human *MSH3* after ASO treatment. Our study shows that ASO-mediated MSH3 reduction can prevent *HTT* CAG repeat expansion in HD 125 CAG iPSC–derived striatal neurons, highlighting the therapeutic potential of this approach.

INTRODUCTION

Huntington's disease (HD) is a fatal neurodegenerative disorder caused by an expanded CAG repeat in the huntingtin gene (*HTT*), with longer inherited alleles initiating an earlier age at disease onset (*1*). Expanded CAG repeat tracts are unstable intergenerationally (*2*–*8*) and somatically (*5*, *6*, *9*–*12*), with somatic cells showing a bias toward expansion in a length-, time-, and tissue-dependent manner (*6*, *10*, *11*, *13*–*16*). The rate of this expansion is affected by cis modifiers, such as interruptions in the repeat sequence (*15*, *17*, *18*), and trans modifiers, most notably DNA repair genes (*17*, *19*). Both classes of modifiers affect somatic expansion rates in blood cells, which in turn correlate with clinical outcomes (*15*). These observations support the idea that HD pathogenesis involves two sequential components. First, the inheritance of an expanded repeat (≥36 CAG), which, upon transcription, replication, or repair, forms secondary structures such as loop-outs that are substrates for further expansion. Second, somatic expansion of the CAG repeats to a length above a toxic pathogenic threshold, which triggers neuronal damage, dysfunction, and eventual neurodegeneration that drives clinical HD features (*20*). It is now widely accepted that therapeutic strategies to reduce somatic expansion could delay onset and slow disease progression in patients with HD.

MSH3 variants have been implicated as modifiers of HD by several genome-wide association studies (GWASs) (*17*, *21*, *22*). MSH3 is a mismatch repair (MMR) protein, which, together with MSH2, forms the MutSβ complex. Although its canonical function is to protect DNA integrity by mainly repairing insertion-deletion loops (*23*–*25*), collective evidence in multiple repeat expansion disorder mouse models, human cell models, and patients suggests that it exerts its modifier effect through somatic expansion via the error-prone repair of abnormal DNA structures at CAG repeats. Lowering MSH3 reduces repeat expansion in mouse models of HD (*26*–*29*), as well as other trinucleotide repeat disorders such as myotonic dystrophy type 1 (DM1; CTG expansions in *DMPK*) (*30*, *31*) and fragile X syndrome (FXS; CGG expansions in *FMR1*) (*32*). This is also seen in human cell models of CTG (*33*–*35*) and GAA (*36*) expansions. In patients with DM1, the *MSH3* single-nucleotide polymorphism (SNP) rs26279, which results in an amino acid change in the adenosine triphosphatase domain, affected somatic instability (*37*). In patients with HD, the *MSH3* haplotype 5AM1 (tagSNP: rs701383) that hastens disease onset was associated with cis–expression quantitative trait loci for increased *MSH3* expression in blood and was enriched in the top 25% of HD gene carriers with the highest proportion of somatic expansions (*17*). Another study identified the leading imputed SNP from the *MSH3/DHFR* signal in the TRACK-HD GWAS to be associated with a three-repeat

[1]Huntington's Disease Centre and Department of Neurodegenerative Disease, UCL Queen Square Institute of Neurology and UK Dementia Research Institute, UCL, London, UK. [2]School of Molecular Biosciences, College of Medical, Veterinary and Life Sciences, University of Glasgow, Glasgow, UK. [3]UK Dementia Research Institute at University of Cambridge and Department of Clinical Neurosciences, University of Cambridge, Cambridge Biomedical Campus, Cambridge CB2 0AH, UK. [4]Department of Molecular Neuroscience, Transylvanian Institute of Neuroscience, 400191 Cluj-Napoca, Romania. [5]Stanley Center for Psychiatric Research, Broad Institute of MIT and Harvard, Cambridge, MA, USA. [6]Ionis Pharmaceuticals, Carlsbad, CA, USA. [7]Department of Genetics and Genomic Medicine, Great Ormond Street Institute of Child Health, London, UK. [8]Department of Genetics, Harvard Medical School, Boston, MA, USA.
†These authors contributed equally to this work.
*Corresponding author. Email: s.tabrizi@ucl.ac.uk

allele (*MSH3 3a*) of a nona-nucleotide tandem repeat sequence within exon 1 of *MSH3* (*38*). This variant was associated with delayed age of disease onset, reduced somatic expansion in both HD and DM1, and slower disease progression in HD (*38*). Although a functional difference between the *MSH3 3a* allele and the most common *MSH3 6a* allele cannot be ruled out, whole-blood RNA sequencing (RNA-seq) indicated that homozygous *MSH3 3a* carriers had reduced *MSH3* expression (*38*), suggesting that this contributes, at least in part, to the reduced somatic expansion observed for individuals carrying these alleles. The same variant, *MSH3 3a*, was later implicated as a modifier of X-linked dystonia parkinsonism (CCCTCT expansions within an *SVA* retrotransposon insertion in *TAF1*), similarly delaying disease onset (*39*). Last, seven patients with HD have been identified with heterozygous loss-of-function mutations in *MSH3*, all of whom had delayed onset, less severe cognitive/motor signs, or both. For those with onset data available, their average age at motor onset was delayed by 10.6 years (*40*, *41*), ultimately validating the efficacy of MSH3 depletion in the target population of patients with HD. Together, these data highlight MSH3 lowering as a potential therapeutic strategy for repeat expansion disorders.

Unlike many other DNA repair genes implicated as modifiers of HD, *MSH3* can tolerate a high degree of loss-of-function variation (*42*, *43*), making it an ideal therapeutic target. The ratio of observed/expected loss-of-function variants in *MSH3* is 0.912 (*44*), which is well above the threshold of 0.6 that typically indicates intolerance of loss of function. Concordant with this, Msh3-deficient mice are not more tumor-prone than their wild-type counterparts, and they demonstrate a normal lifespan (*45*, *46*). Mutations in other members of the MMR network typically cause genetic colorectal cancer syndromes in patients (*47*–*55*), whereas *MSH3* mutations are generally well tolerated (*44*). This excludes some extremely rare cases, reported only in 16 individuals to date, whereby germline biallelic *MSH3* mutations were shown to associate with colorectal adenomas, which if left untreated can lead to cancer (*56*–*60*). The lower risk of carcinogenesis in the absence of MSH3 compared with most other MMR proteins is likely explained by functional redundancy for the repair of base mismatches with the more abundant MSH6 (*61*, *62*). In addition, MSH3's specific substrate, small insertion-deletion loops, are less oncogenic. No links between MSH3 dysfunction and central nervous system (CNS)–derived tumors have been made in humans (*63*). This is supported by recent HD mouse data whereby injection of *MSH3* small interfering RNAs, which are primarily retained in the CNS, resulted in no detectable impact on CNS mononucleotide repeat instability at 12 weeks postinjection (*28*). Together, these data suggest that lowering MSH3 in the brain appears to be safe.

Antisense oligonucleotides (ASOs) are short nucleic acids, chemically modified to bind to RNA by Watson-Crick base pairing, leading to subsequent degradation of the RNA target. They have been shown to be effective in numerous animal models and patients with a wide range of diseases (*64*, *65*), with six so far having been approved for neurological disease (*66*, *67*). Given the technical challenges of targeting gene expression in patient brains, particularly in deep-brain structures like the striatum (*61*, *62*), it is important to investigate the degree of MSH3 lowering by ASOs that may be required to have a clinical benefit.

Here, we examined the effect of MSH3 lowering by ASO on CAG repeat instability in induced pluripotent stem cell (iPSC)–derived striatal neurons from a patient with HD. The effect of knocking out Fanconi anemia-associated nuclease 1 (FAN1), the most significant modifier of HD age at onset (*17*), on the somatic instability outcomes of MSH3 lowering was also explored. In addition, the transcriptional signature associated with ASO-mediated *MSH3* lowering was examined through both bulk and single-nuclei RNA-seq (snRNA-seq) approaches. Last, we describe the generation of a knock-in mouse model expressing the human *MSH3* gene, which will be important for evaluating human *MSH3*-targeting molecules in the future.

RESULTS

MSH3 ASO treatment results in dose-dependent MSH3 knockdown in HD iPSC–derived striatal neurons

Approximately 230 gapmer ASOs, complementary to human *MSH3* mRNA and designed to silence gene expression via RNaseH1-mediated degradation, were developed by Ionis Pharmaceuticals Inc. ASOs were screened in A-431 cells at 2 μM, using quantitative reverse transcription polymerase chain reaction (qRT-PCR) to assess *MSH3* expression after 24 hours of ASO treatment. The top six *MSH3* ASOs were selected for further evaluation on the basis of their potent activity for *MSH3* suppression in A-431 cells (table S1 and fig. S1). The most potent of these ASOs, herein referred to as the *MSH3* ASO, was taken forward for further in vitro and in vivo studies.

Striatal medium spiny neurons are the most vulnerable cell type in HD brains, and, thus, we sought to assess the effect of *MSH3* lowering in postmitotic human striatal cultures enriched for medium spiny neurons. We differentiated an iPSC line derived from a patient with HD carrying 125 CAG repeats in exon 1 of *HTT* into medium spiny-enriched striatal neurons using the Arber *et al.* (*68*) protocol (Fig. 1A). Consistent with previous reports, immunocytochemistry showed that cultures were 86% ± 4 neuronal [microtubule-associated protein 2 $(MAP2)^+$], 67% ± 13 striatal neuron identity [$MAP2^+$, forkhead box protein 1 $(FOXP1)^+$], and 30% ± 4 medium spiny neurons [$MAP2^+$, $FOXP1^+$, dopamine- and cyclic–adenosine 5′-monophosphate–regulated phosphoprotein $(DARPP32)^+$] (Fig. 1A) (*68*, *69*). These cultures were treated at day 36 (baseline) with the *MSH3* ASO for 1 week. To determine the cellular uptake of the *MSH3* ASO, they were then probed with an antibody that selectively binds to the phosphorothioate backbone of the ASO, demonstrating efficient gymnotic uptake by striatal neurons ($FOXP1^+$, $MAP2^+$; Fig. 1B). A dose titration was also performed, which determined the doses required to achieve ~25, ~50%, and maximal non-toxic MSH3 knockdown to be 0.022, 0.26, and 3 μM, respectively [Fig. 1C, median inhibitory concentration (IC_{50}) = 0.255, coefficient of determination (R^2) = 0.75]. In addition, the effect of MSH3 lowering on the abundance of other MutS components (MSH2 and MSH6) was examined, with no changes detected (Fig. 1D). To assess the effect of long-term *MSH3* ASO treatment on *MSH3* lowering in our striatal neurons, we quantified *MSH3* transcript and protein over time. We observed continued dose-dependent knockdown of both *MSH3* transcript and protein (Fig. 1E, IC_{50} = 0.137, R^2 = 0.75; Fig. 1F) and found no changes in cell viability at 9 or 15 weeks of treatment (fig. S2). Together, these data show that the selected *MSH3* ASO successfully lowered *MSH3* in HD iPSC–derived striatal cultures enriched for the most vulnerable neuronal type in HD without overt toxicity.

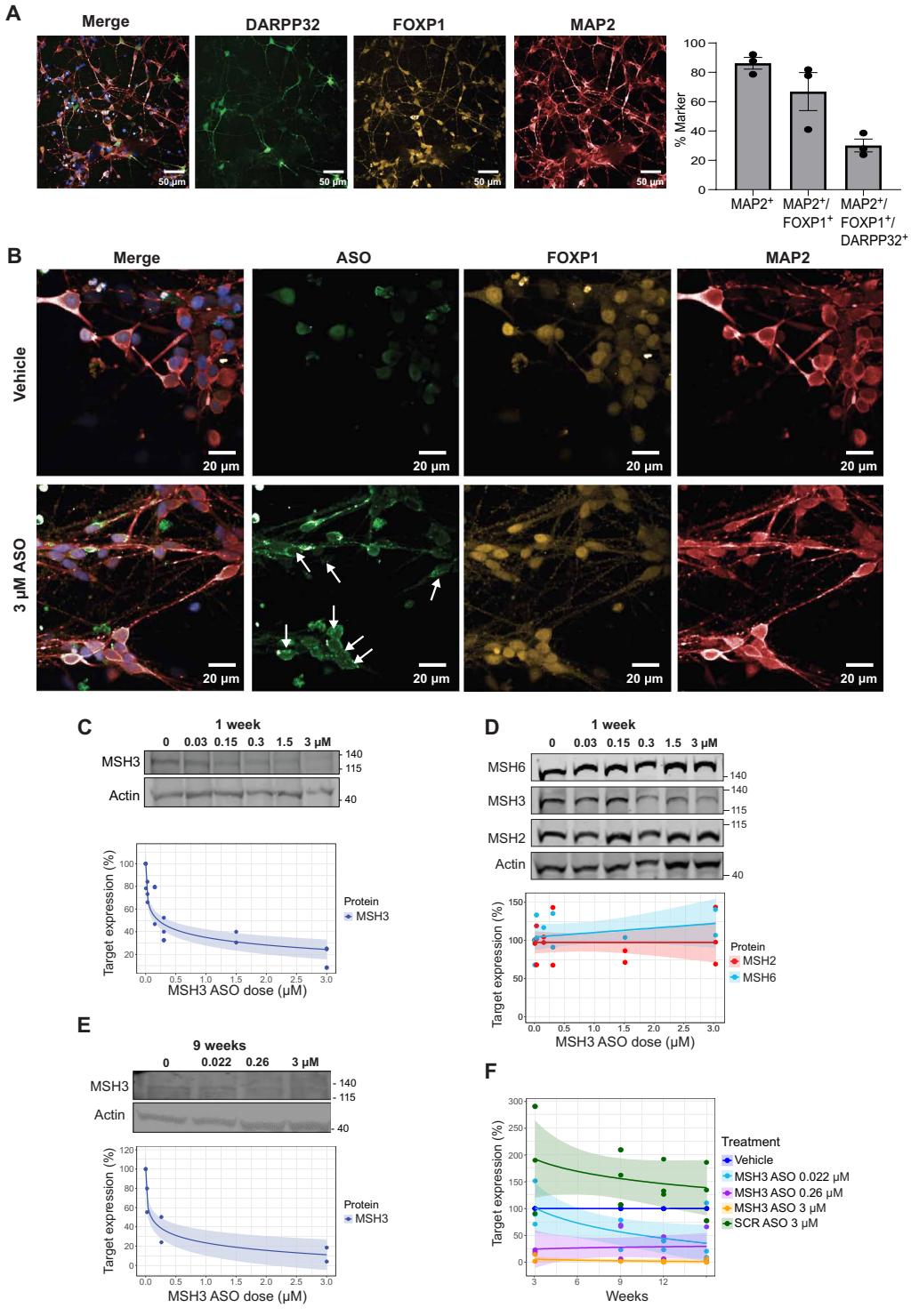

Fig. 1. *MSH3* lowering in HD iPSC–derived striatal neurons with an *MSH3* ASO. (**A**) Shown is immunofluorescent staining of HD 125 CAG iPSC–derived striatal neurons after 36 days of differentiation. Costaining of cultured neurons for DARPP32 (green), FOXP1 (orange), MAP2 (red), and Hoechst 33342 counterstain (blue, nuclei) indicates that the cultures were enriched for medium spiny neurons. Marker-positive cell frequency for MAP2, FOXP1, and DARPP32 as a proportion of the total number of cells counterstained with Hoechst was quantified. (**B**) Immunofluorescent staining is shown for HD 125 CAG iPSC–derived striatal neurons treated for 1 week with *MSH3* ASO (green; white arrows indicate ASO foci): FOXP1 (orange), MAP2 (red), and Hoechst 33342 (blue). (**C** to **E**, top) Representative Western blots showing MSH3 [(C) to (E)], and MSH2 and MSH6 (D) in response to 1 week or 9 weeks of *MSH3* ASO treatment. [(C) to (E), bottom] Quantification of MSH3, MSH2, and MSH6 protein, normalized to actin and presented relative to the vehicle-treated control (PBS) ($n = 2$ or 3, $N = 3$). (**F**) qRT-PCR was used to measure *MSH3* mRNA at each time point throughout the ASO treatment period. *n*, biological replicates, i.e., number of differentiated clones sampled; *N*, technical replicates, i.e., number of samples taken from each differentiated clone at each time point.

MSH3 lowering results in a dose-dependent reduction of CAG repeat expansion in HD iPSC–derived striatal neurons

To predict the degree of MSH3 knockdown required to slow somatic CAG repeat expansion by 50%, we measured the effect that long-term dose titration of MSH3 in our striatal neurons had on CAG repeat length over time. Cells were treated at day 36 and cultured continuously in ASO-containing medium for 15 weeks, with samples collected every 3 weeks to assess CAG repeat length. We observed a dose-dependent slowing of CAG repeat expansion after *MSH3* ASO treatment with maximal MSH3 lowering ablating repeat expansions ($\beta = -0.023$ CAG/week ± 0.015, $P = < 0.001$), whereas the scrambled ASO control did not affect CAG repeat expansion rate (Fig. 2, A to C, and fig. S3).

To examine the effects in cells completely lacking MSH3, we used CRISPR-Cas9 to generate 125 CAG *MSH3*$^{-/-}$ iPSC clones (Fig. 2D and fig. S4). Similar to the effects of the *MSH3* ASO, genetic *MSH3* knockout did not lead to changes in MSH2 or MSH6 protein abundance (Fig. 2E). These iPSC clones were differentiated into medium spiny-enriched striatal neurons, alongside those derived from 125 CAG unedited iPSCs, which had undergone the CRISPR editing process with no editing (unedited 125 CAG CRISPR control), and CAG repeat expansion was measured for 12 weeks after baseline (Fig. 2, F to H, and fig. S5). Whereas the CAG repeat in unedited striatal neurons expanded over time (Fig. 2, F to H, $\beta = 0.089$ CAG/week ± 0.01), *MSH3*$^{-/-}$ striatal neurons showed ablation of CAG expansions and net contractions of the repeat, with a linear regression trend line that had a significantly nonzero slope (Fig. 2, F to H, $\beta = -0.033$ CAG/week ± 0.01, $P < 0.001$).

To determine the dose-dependence of the effect, MSH3 protein abundance was then plotted against CAG repeat instability rates for all *MSH3* ASO treatments in unedited iPSC-derived striatal neurons, as well as rates for *MSH3*$^{-/-}$ iPSC–derived striatal neurons (Fig. 2I). The fitted curve predicted that ~41% MSH3 lowering was sufficient to reduce the rate of somatic expansion by 50% and that ~83% MSH3 lowering completely prevented net CAG repeat expansions. MSH3 lowering beyond this point appeared to cause net CAG repeat contractions. These data show that lowering MSH3 using an ASO treatment was able to reduce CAG repeat expansion in a dose-dependent manner in striatal neurons, with complete loss of MSH3 ablating repeat expansion and leading to net contraction of the CAG repeat over time.

Maximal ASO-mediated MSH3 lowering prevents CAG repeat expansion in FAN1-deficient HD iPSC–derived striatal neurons

FAN1 is the most significant genetic modifier of age of disease onset in HD, with variants advancing onset by up to 5.2 years (*17*, *19*). Its expression has been shown to protect against CAG repeat expansion in HD cell models, with loss of FAN1 doubling *HTT* CAG expansion rates (*70*, *71*). Owing to the small absolute change in CAG length over the 15-week period in our 125 CAG iPSC–derived striatal neurons (~1.2 CAGs total), we additionally sought to establish the effect of MSH3 lowering in a rapidly expanding repeat system. If MSH3 lowering successfully slowed CAG repeat expansion in *FAN1*$^{-/-}$ striatal neurons, it could be an effective therapy even in individuals with high polygenic risk from genetic variants that promote somatic expansion. CAG expansion assays were therefore repeated in medium spiny-enriched striatal neurons generated from a 125 CAG *FAN1*$^{-/-}$ iPSC line (fig. S4) treated with the maximal dose of the *MSH3* ASO (3 μM) (Fig. 3, A to C). For these cultures, linear regression analyses determined slopes for vehicle ($\beta = 0.254$ CAG/week ± 0.06, $P < 0.001$; Fig. 3B) and 3 μM scrambled ASO treatment ($\beta = 0.336$ CAG/week ± 0.11, $P < 0.001$; Fig. 3B) to be significantly nonzero, demonstrating repeat expansion over time (Fig. 3, A to C, and fig. S6). Conversely, treatment with 3 μM *MSH3* ASO was not significantly different to a zero slope ($\beta = -0.054$ CAG/week ± 0.08, $P = 0.78$; Fig. 3B), demonstrating that maximal *MSH3* lowering prevented CAG repeat expansion, even in a rapidly expanding system (Fig. 3, A to C). These experiments were performed in conjunction with medium spiny-enriched striatal neurons derived from 125 CAG iPSCs that had undergone the CRISPR process without editing as a control. Treatment of these cultures with 3 μM *MSH3* ASO replicated the data presented in Fig. 2A, showing that *MSH3* ASO treatment ablated CAG repeat expansion ($\beta = -0.02$ CAG/week ± 0.02; Fig. 3, D to F, and fig. S7). Together, these data demonstrate that *MSH3* lowering stopped CAG repeat expansion even in striatal neurons lacking FAN1.

Large repeat expansions have been observed in postmortem brain tissues of patients with HD (*10*), even before disease onset, and are more common in patients with HD with early disease onset (*14*). However, these events are difficult to detect by bulk fragment length analysis because of bias toward amplification and detection of shorter and more common alleles and relative insensitivity to rare alleles. Small-pool PCR was therefore used to detect rare, large expansion or contraction events in the CAG tract of the mutant *HTT* allele. *FAN1*$^{-/-}$ striatal neuronal cultures treated with vehicle or scrambled ASO exhibited expansions of up to 403 CAG repeats and contractions down to 120 CAG repeats (Fig. 3G). Although differences between scrambled and *MSH3* ASO treatment did not reach significance, quantifying the frequency of these rare expansion events reflected the same pattern as in bulk fragment analysis measures. That is, large expansions were observed at similar frequencies with scrambled ASO and vehicle treatments, but *MSH3* ASO treatment tended to suppress their occurrence (vehicle versus *MSH3* ASO: mean difference = 0.324 expansions per lane ± 0.155, $P = 0.0692$; Fig. 3H). Large expansions were also detectable in unedited striatal neuronal cultures (fig. S8A), mirroring what is seen in postmortem brain tissue of a patient with HD (*10*, *14*). However, over the 12-week period assessed, these events occurred infrequently, and, hence, differences between conditions were not measurable for the unedited cells (fig. S8B). Collectively, these findings highlight the relevance of HD iPSC–derived medium spiny neuron–enriched striatal cultures as a model for studying the biology of CAG repeat dynamics, reflecting the patterns observed in postmortem brain tissue of a patient with HD, and suggest that MSH3 may exert additional influence on the occurrence of large, rare expansion events.

Transcriptional changes associated with *MSH3* lowering reveal no dysregulation of DNA repair pathways in HD iPSC–derived striatal neurons

To assess the transcriptional signature of MSH3 lowering, we performed bulk RNA-seq on striatal neurons treated for 2 weeks from baseline (day 36) with vehicle, scrambled ASO (3 μM), or one of three *MSH3* ASOs (3 μM): *MSH3* ASO-1 (used in all prior experiments), *MSH3* ASO-2, and *MSH3* ASO-3 (see Materials and Methods). As expected, *MSH3* abundance was reduced by all three *MSH3* ASOs compared with vehicle, whereas the scrambled ASO showed no effect (Fig. 4A). A stepwise reduction in *MSH3* read counts was observed after treatment with ASO-3 (reduced to 20% ± 9.0 of vehicle, $P < 0.001$), ASO-2 (reduced to 10.2% ± 1.9 of vehicle,

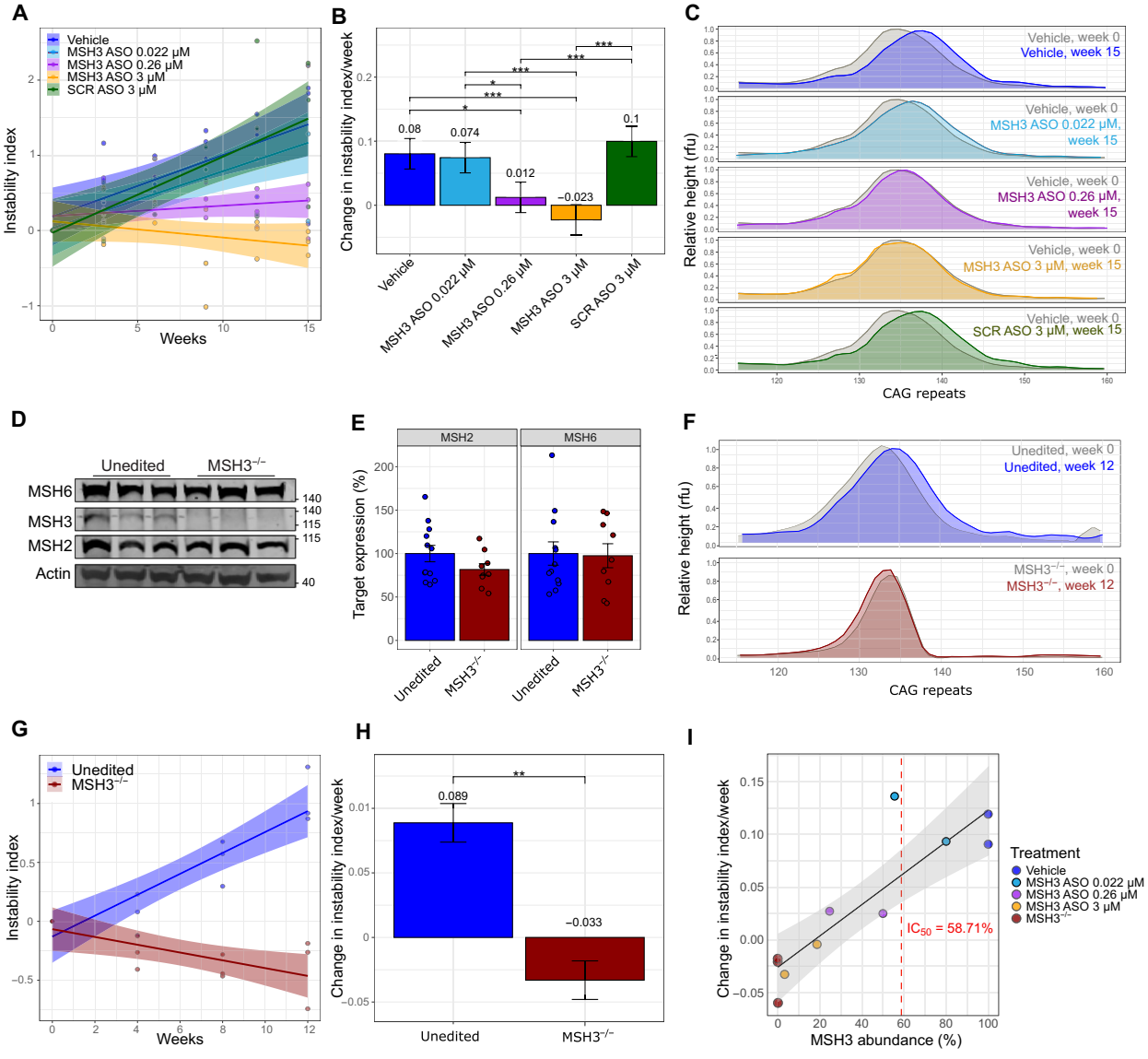

Fig. 2. Fragment analysis to assess the effect of MSH3 lowering on CAG repeat instability in HD iPSC–derived striatal neurons. (**A**) Changes in CAG repeat length over time were assessed in HD 125 CAG iPSC–derived striatal neurons treated with different doses of *MSH3* ASO (0.022 μM, light blue; 0.26 μM, purple; 3 μM, orange) as well as vehicle control (PBS, dark blue) and 3 μM scrambled ASO control (SCR, green). Each data point shows an independent biological replicate ($n = 4$), calculated from the mean of three technical replicates ($N = 3$). The shaded regions indicate 95% confidence intervals. (**B**) The rate of change in CAG repeat length per week was determined from a linear mixed-effects model [lmer(instability_metric ~ treatment * time + (1 + time | differentiation)] by the estimated marginal means method, with differences between conditions adjusted for multiple testing using the Bonferroni method ($n = 4$, $N = 3$). (**C**) Representative fragment length traces (normalized to modal peak height): Baseline (gray); 15 weeks of treatment with vehicle (dark blue); 15 weeks of treatment with 0.022 μM (light blue), 0.26 μM (purple), or 3 μM *MSH3* ASO (orange); or 15 weeks of treatment with 3 μM scrambled ASO (SCR, green). (**D**) Representative Western blots of MSH3, MSH2, and MSH6 after CRISPR-Cas9 editing to knock out *MSH3* in HD 125 CAG iPSCs. Each lane shows a separate clone. (**E**) Quantification of MSH2 and MSH6 protein in *MSH3*$^{-/-}$ iPSC clones, normalized to actin, and presented relative to the mean for unedited cells ($n = 9$ to 12, $N = 1$). (**F**) Representative fragment length traces (normalized to modal peak height) of HD iPSC–derived striatal neurons: Baseline (gray), 125 CAG unedited iPSC–derived striatal neurons at 12 weeks (blue), and 125 CAG *MSH3*$^{-/-}$ iPSC–derived striatal neurons at 12 weeks (dark red). (**G**) Effect of *MSH3* knockout on CAG length over time in HD iPSC–derived striatal neurons is shown. Each data point shows an independent biological replicate ($n = 3$), calculated from the mean of three technical replicates ($N = 3$). The shaded regions indicate the 95% confidence intervals. (**H**) The rate of change in CAG length per week was determined from a linear mixed-effects model [lmer(instability_metric ~ treatment * time + (1 + time | differentiation)] by the estimated marginal means method ($n = 3$, $N = 3$). (**I**) Regression analysis of the relationship between MSH3 protein abundance and CAG expansion rate in HD 125 CAG iPSC–derived striatal neurons treated with vehicle or different doses of ASO or lacking *MSH3* altogether (*MSH3*$^{-/-}$). MSH3 protein abundance was determined by densitometry of Western blots, and instability rates represent the change in instability index per week, relative to the baseline sample for each differentiation, clone, and genotype. Data points are colored according to treatment group and genotype; vehicle and *MSH3* ASO dosing groups comprised unedited HD 125 CAG iPSC–derived striatal neurons. The black line represents the fitted regression. The shaded region indicates the 95% confidence intervals. The IC_{50} is depicted by a red dashed vertical line at an MSH3 protein abundance of 58.7% of that for the vehicle group. The IC_{50} was calculated from the regression model coefficients and represents the MSH3 protein abundance at which the CAG expansion rate was halved. ***$P < 0.001$, **$P < 0.01$, and *$P < 0.05$. *n*, biological replicates, i.e., differentiation of each clone; *N*, technical replicates, i.e., number of samples taken from each differentiation culture at each time point.

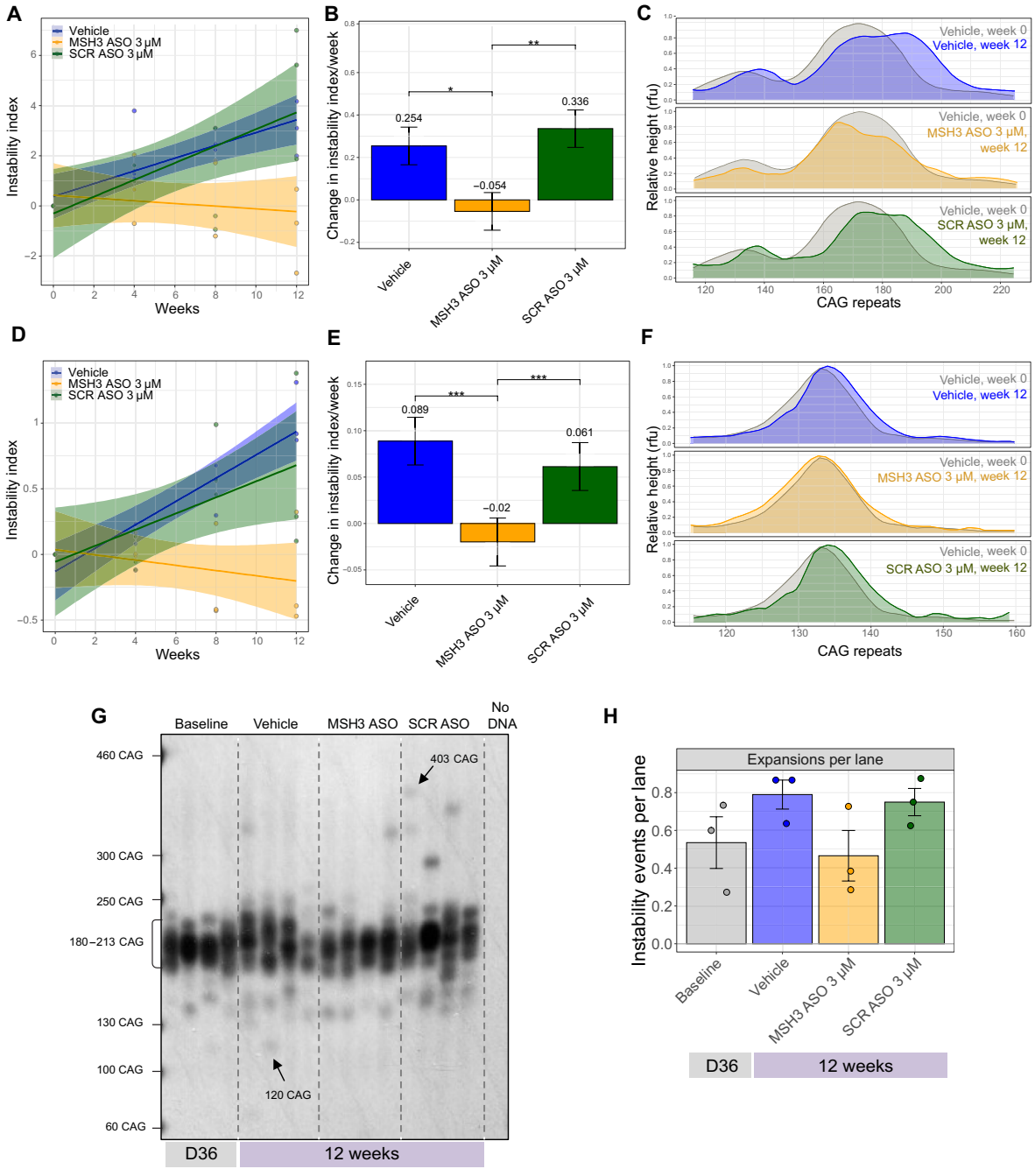

Fig. 3. The effects of MSH3 lowering on CAG repeat instability in *FAN1*$^{-/-}$ HD iPSC–derived striatal neurons. (**A** to **C**) Shown are CAG repeat length changes in *FAN1* $^{-/-}$ HD 125 CAG iPSC–derived striatal neurons treated with *MSH3* ASO or scrambled (SCR) ASO ($n = 4$, $N = 3$). (**D** to **F**) Shown are CAG repeat length changes in 125 CAG unedited iPSC–derived striatal neurons treated with *MSH3* ASO or scrambled ASO ($n = 3$, $N = 3$), which were derived from a 125 CAG iPSC clone that had undergone CRISPR editing but with no successful cutting. [(A) and (D)] Change in CAG repeat length over time in striatal neurons treated with vehicle (PBS, blue), 3 μM *MSH3* ASO (orange), and 3 μM scrambled ASO (SCR, green). Each data point shows an independent biological replicate ($n = 3$ or 4), calculated from the mean of three technical replicates ($N = 3$). The shaded regions indicate 95% confidence intervals. [(B) and (E)] The rate of change in CAG repeat length per week was determined from a linear mixed-effects model [lmer(instability_metric ~ treatment * time + (1 + time | differentiation)] by the estimated marginal means method, with differences between conditions adjusted for multiple testing using the Bonferroni method. [(C) and (F)] Representative fragment length traces (normalized to modal peak height): Baseline (day 36 of differentiation, gray), 12 weeks of treatment postbaseline with vehicle (blue), 3 μM *MSH3* ASO (orange), and 3 μM scrambled ASO (SCR, green). (**G**) Small-pool PCR was used to measure the effect of *MSH3* ASO treatment on large, rare repeat expansion events in *FAN1*$^{-/-}$ 125 CAG iPSC–derived striatal neurons at baseline (day 36 of differentiation, D36) or after treatment with vehicle, scrambled (SCR) ASO, or *MSH3* ASO for 12 weeks postbaseline ($n = 3$, $N = 3$, with 16 separate PCRs assessed per sample). The length of the most extreme alleles was measured using GelAnalyzer. (**H**) Frequency of large repeat expansions per lane, with large expansions defined as those falling outside the modal spread of alleles. Each data point shows an independent biological replicate. *n*, biological replicates, i.e., differentiation of each clone; *N*, technical replicates, i.e., number of samples taken from each differentiation culture at each time point. ***$P < 0.001$, **$P < 0.01$, and *$P < 0.05$.

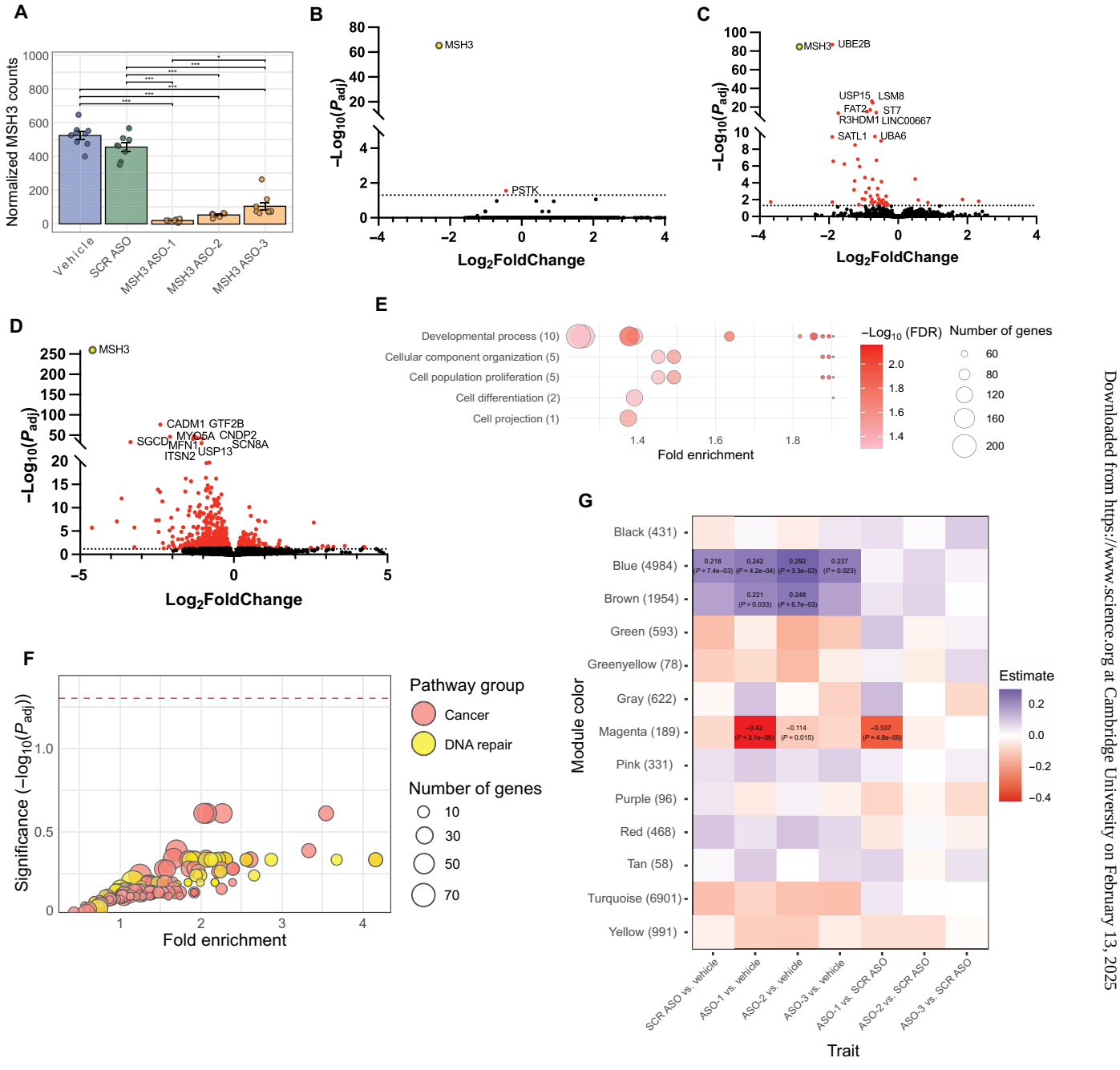

Fig. 4. Assessment of *MSH3* ASO treatment on the global transcriptome by bulk RNA-seq in HD iPSC–derived striatal neurons. (**A**) Shown are normalized read counts of *MSH3* in HD 125 CAG iPSC–derived striatal neurons treated with vehicle (blue); scrambled ASO (green); and *MSH3* ASO-1, *MSH3* ASO-2, or *MSH3* ASO-3 (orange). (**B** to **D**) Volcano plots of DEGs (red) and non-DEGs (black) for 125 CAG iPSC–derived striatal neurons treated with *MSH3* ASOs versus scrambled (SCR) ASO: (B) *MSH3* ASO-3; (C) *MSH3* ASO-2; and (D) *MSH3* ASO-1. The horizontal black dashed line represents adjusted P (P_{adj}) = 0.05 significance. The top 10 DEGs are labeled, with *MSH3* highlighted in yellow. The full list of DEGs is available in data file S1. (**E**) Shown are nodal pathway plots summarizing pathways dysregulated in 125 CAG iPSC–derived striatal neurons treated with *MSH3* ASO-1 versus scrambled (SCR) ASO. The size of the bubble depends on the number of genes enriching the GO term. The full details for the GO enriched terms are available in data file S2. (**F**) Cancer and DNA repair gene set enrichment analysis of DEGs from 125 CAG iPSC–derived striatal neurons treated with *MSH3* ASO-1 compared with scrambled (SCR) ASO. Pathways related to cancer and DNA repair were extracted from GO and KEGG databases (data file S3). Fold enrichment was plotted against enrichment significance (−$\log_{10} P_{adj}$), with a red dashed horizontal line indicating the threshold for significance (P_{adj} = 0.05). *MSH3* ASO-2 and *MSH3* ASO-3 were excluded from the figure because of insufficient DEGs for analysis (ASO-3) or a lack of significant results (ASO-2). (**G**) Heatmap shows correlation of WGCNA gene expression modules with *MSH3* ASO or scrambled (SCR) ASO treatment compared with vehicle in iPSC-derived striatal neurons. Modules on the *y* axis are ranked by their significance, with arbitrary colors assigned as names for each module and numbers in brackets indicating gene counts. The color of tiles within the heatmap reflects the correlation strength and direction between each module's gene signature and the treatment, with red indicating negative and blue indicating positive. Correlation coefficients and *P* values are displayed when significant. Full details are in data file S4. ***$P < 0.001$, **$P < 0.01$, and *$P < 0.05$.

$P < 0.001$), and ASO-1 (reduced to 3.9% ± 1.5 of vehicle, $P < 0.001$). To compare transcriptional signatures of the three *MSH3* ASOs with scrambled ASO and vehicle control, we undertook differential gene expression analyses, pathway enrichment, and weighted gene coexpression network analysis (WGCNA).

There were 5290 differentially expressed genes (DEGs) between scrambled ASO and vehicle conditions, 2740 of which were down-regulated (fig. S9A). These DEGs are suggestive of ASO chemistry effects. To control for this and to examine the impact of MSH3 reduction, we compared each of the *MSH3* ASO treatments with scrambled ASO. There were only two DEGs, both down-regulated, between scrambled ASO and *MSH3* ASO-3, one of which was *MSH3* (Fig. 4B). Treatment with *MSH3* ASO-2 resulted in 53 DEGs, 48 of which were down-regulated (Fig. 4C), and *MSH3* ASO-1 treatment resulted in 781 DEGs, 583 of which were down-regulated (Fig. 4D). The full list of DEGs is provided in data file S1, including those for each *MSH3* ASO in comparison with vehicle (fig. S9, B to D).

We performed Gene Ontology (GO) enrichment analysis and then grouped pathways into functional nodes. The effects of ASO chemistry (scrambled ASO versus vehicle) revealed dysregulation of pathways that converged on RNA and protein metabolism, cellular localization, and structural organization (fig. S9E). GO enrichment analyses for *MSH3* ASO-2 and *MSH3* ASO-3 either returned no significant hits [false discovery rate (FDR) > 0.05] or had insufficient DEGs to perform such analysis. The effect of *MSH3* ASO-1 compared with scrambled ASO largely converged on terms related to cell development and structure and cell projection (Fig. 4E). The full details of the enriched GO terms are provided in data file S2. In addition, we assessed whether *MSH3* lowering by these ASOs influenced DNA damage response or cancer pathways (data file S3). We found that these pathways were not significantly disrupted by *MSH3* lowering (Fig. 4F), even with ASO-1 achieving more than a 95% reduction in *MSH3*.

Next, we performed WGCNA, a method that identifies clusters (modules) of genes with highly correlated expression patterns. This approach allows for the detection of potential coregulated or functionally related genes by grouping them into modules in a holistic and unbiased manner (Fig. 4G and data file S4). Compared with vehicle, scrambled ASO treatment correlated positively with the expression pattern of the blue module, which showed enrichment for ribosomal and mitochondrial pathways (data file S4). When compared with vehicle, all three *MSH3* ASOs replicated this effect. In addition, all four ASOs, including scrambled, up-regulated the brown module, which was enriched for pathways related to the plasma membrane and structural activity (data file S4). Although after FDR correction this up-regulation of the brown module was only statistically significant for ASO-1 ($P = 0.033$) and ASO-2 ($P = 0.0067$), the consistent transcriptional pattern across all four ASO molecules suggests a common effect attributable to ASO chemistry.

Comparing *MSH3* ASOs with scrambled ASO treatment, the only association was with the magenta module, which was down-regulated specifically by *MSH3* ASO-1. This module was enriched for synaptic membrane proteins and morphogenesis proteins. Because this effect was not seen with other similarly potent *MSH3* ASOs, we considered whether an ASO sequence–specific effect, such as off-target knockdown, could be driving it. We examined the gene expression profiles of the predicted off-target loci for *MSH3* ASO-1; within our dataset, 9 of the 18 predicted off-target loci were annotated (fig. S10). Of those, two were down-regulated: *ATG5* ($P = 8.89 \times 10^{-28}$) and *EYS* ($P = 1.98 \times 10^{-5}$). These genes are members of pathways involved in cell projection, cell development, system development, and cell differentiation, potentially accounting for down-regulation of the magenta module.

snRNA-seq of *MSH3* ASO–treated HD iPSC–derived striatal neuronal cultures

We next undertook snRNA-seq to investigate whether the *MSH3* ASO-1 treatment had cell type–specific effects or affected the composition of cells in our striatal neuronal cultures. We compared 125 CAG HD iPSC–derived striatal neuronal cultures treated with either *MSH3* ASO-1 (3 μM) or scrambled ASO (3 μM) for 12 weeks postbaseline. To reduce the complexity of this large dataset while preserving its intrinsic structure, we used Uniform Manifold Approximation and Projection (UMAP). We then used Leiden unsupervised clustering to identify groups of similar cells on the basis of their gene expression profiles. Five clusters were identified, all of which were present in similar proportions in both *MSH3* and scrambled ASO treatment groups (Fig. 5A). No clusters were specific to either treatment group, suggesting that *MSH3* ASO treatment did not affect culture composition, either through influencing cell fate or causing toxicity (Fig. 5, B and C). *MSH3* ASO treatment reduced *MSH3* abundance (Fig. 5D) and resulted in fewer cells expressing *MSH3* in all clusters (fig. S11), suggesting that the ASO entered and engaged its target in all cell types within the culture.

Differential expression analysis of these snRNA-seq data replicated findings from bulk RNA-seq. *MSH3* ASO-1 treatment was once again associated with significant down-regulation of pathways involved in synaptic structures and neuronal development ($P < 0.01$; Fig. 5, E and F). To determine whether differential expression was cell-state specific, each cell was scored by its expression of the 20 genes most down-regulated by *MSH3* ASO treatment. This involved summing their expression and comparing with the sum of 5000 control genes. Scores were consistently lower for all *MSH3* ASO–treated clusters compared with scrambled ASO–treated clusters (Fig. 5G). This suggests that the down-regulation of synaptic genes within our medium spiny neuron–enriched cultures, which we believe to be off-target driven effects, were not cell-state specific.

MSH3 ASO-1 ICV delivery reduces *MSH3* in the brains and spinal cords of humanized *MSH3* knock-in mice

Even when ASOs share the same chemical modifications and target the same gene, their safety and efficacy can vary greatly depending on the RNA sequence they target. Factors such as sequence accessibility, off-target effects, binding strength, and the efficiency of target degradation all contribute to this variability, as demonstrated by our RNA-seq analysis. To enable preclinical evaluation of ASO activity on the human *MSH3* gene in vivo, we developed a knock-in mouse model incorporating exons 2 to 10 of the human *MSH3* gene, regulated by the endogenous mouse *Msh3* promoter (fig. S12A). As proof of concept, we tested *MSH3* ASO-1, our most potent tool compound. Bolus intracerebral ventricular (ICV) injection of ASOs into the lateral ventricles of mouse brains is an efficient method of ASO delivery (*72*). Human *MSH3* knock-in mice were treated with *MSH3* ASO-1 via ICV, and brain and spinal cord tissues were harvested 14 days later (fig. 12B). Injection with vehicle [phosphate-buffered saline (PBS)] or a scrambled ASO control showed no change in MSH3 expression (Fig. 6 and fig. S12C). The *MSH3* ASO resulted in a dose-dependent reduction of *MSH3* mRNA across all brain regions tested, with the maximal dose of 30 μg leading to a 49% reduction in the

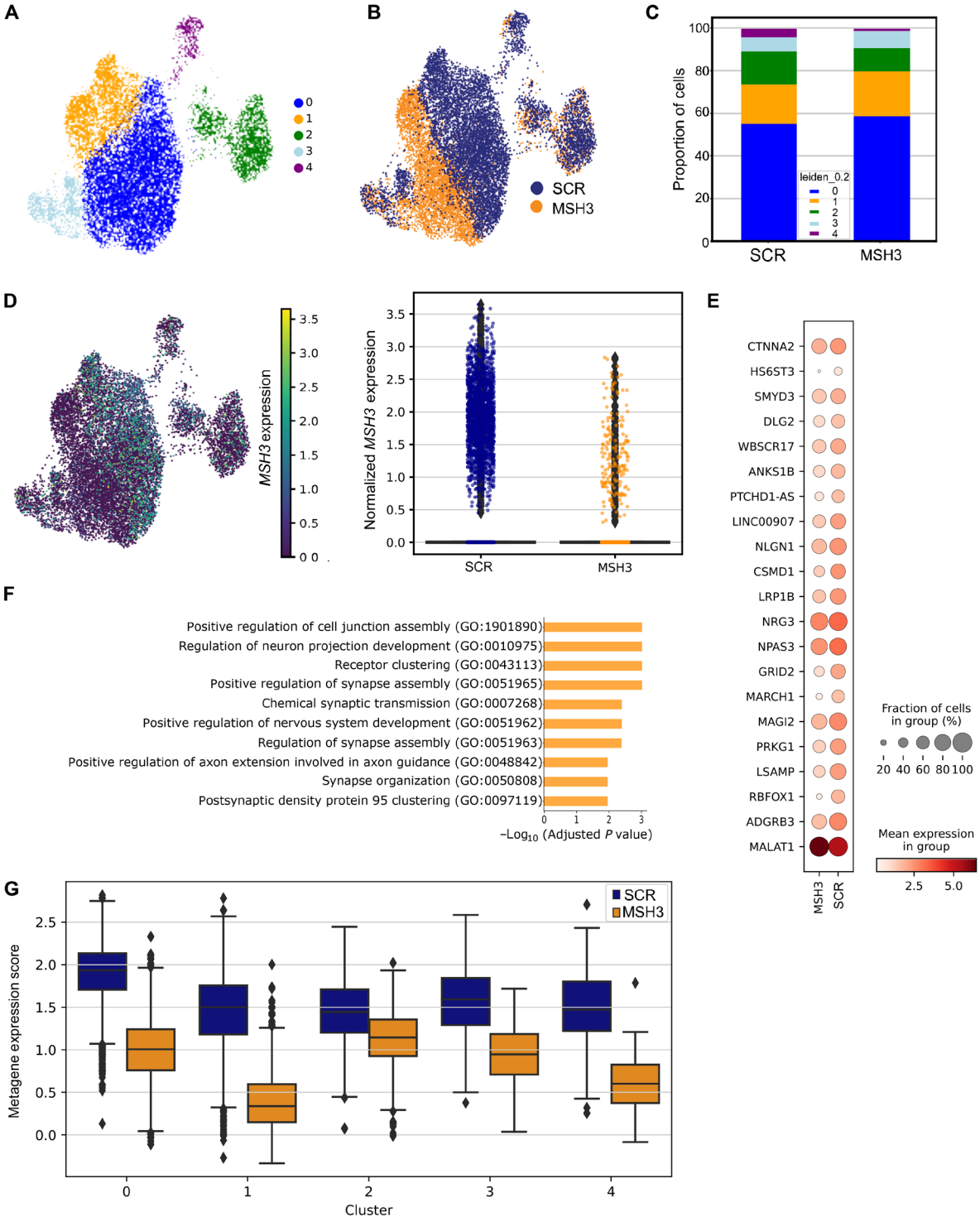

Fig. 5. snRNA-seq reveals no cell type–specific effects of *MSH3* ASO treatment. (**A** and **B**) UMAPs of snRNA-seq data from 125 CAG iPSC–derived striatal neurons subjected to Leiden unsupervised clustering (A) and after *MSH3* ASO or scrambled (SCR) ASO treatment (B). (**C**) Bar plot shows proportion of cells from each treatment category in each cluster. (**D**, left) UMAP labeled by *MSH3* expression; (D, right) jitter plot displaying *MSH3* expression. In both cases, *MSH3* expression was normalized for library size and log1p transformed. (**E**) Dot plot of top DEGs between *MSH3* ASO and scrambled (SCR) ASO treatments. (**F**) Gene set enrichment for down-regulated genes after treatment with *MSH3* ASO. (**G**) Distribution of per-cell differential expression effect of *MSH3* ASO treatment across Leiden clusters.

cortex ($P < 0.001$), a 46% reduction in the striatum ($P < 0.001$), a 77% reduction in the brainstem ($P < 0.001$), and a 74% reduction in the spinal cord ($P < 0.001$) (Fig. 6). The ASO was well tolerated at the doses tested, as evidenced by normal home cage behavior and no motor abnormalities at the 2-week necropsy time point (table S2). Staining of mouse whole brain and spinal cord revealed no signs of neurodegeneration, as assessed by calbindin expression (fig. S12D). These data show in vivo target engagement of the *MSH3* ASO-1 in multiple brain regions, including the striatum and cortex, which show vulnerability in HD, and demonstrate that suppression of *MSH3* was well tolerated in the human *MSH3* knock-in mice.

DISCUSSION

Establishing the degree of MSH3 reduction required for therapeutic benefit is vital to inform future clinical development strategies in patients. We explored this using human medium spiny neuron–enriched striatal cultures derived from the 125 CAG HD iPSC cell line, treated with an ASO targeting human *MSH3* (*MSH3* ASO-1). We demonstrated that HD striatal neurons successfully took up *MSH3* ASO and that MSH3 lowering led to a dose-dependent reduction in somatic CAG expansion in the *HTT* gene. Lowering MSH3 by 41% was sufficient to halve the somatic expansion rate, and 83% MSH3 lowering was estimated to completely halt expansion. Further, MSH3 knockdown and knockout appeared to result in net contractions of the *HTT* CAG repeat. Maximal MSH3 lowering (89%) with the *MSH3* ASO was effective at halting bulk somatic expansions, even in human *FAN1*$^{-/-}$ iPSC–derived striatal neurons that showed faster CAG repeat expansion, and additionally reduced the frequency of rare, large expansion events.

The effect of MSH3 reduction on slowing somatic CAG expansion in the *HTT* gene has been well described in rodent and engineered cell models (*26*–*28*, *32*). However, only four previous studies have investigated the dose dependence of this effect in HD, all of which were conducted using mouse models (*26*, *28*, *29*, *73*). We replicated these findings in HD iPSC–derived striatal cultures enriched for medium spiny neurons, showing dose-dependent slowing of CAG expansion with lowering of MSH3. In addition, we expanded on the scope of previous studies by including five different levels of *MSH3* knockdown, improving the granularity of dose titration to support future clinical trial design. Moreover, we demonstrated that MSH3 lowering remained effective at ablating somatic expansions even in *FAN1*$^{-/-}$ striatal neurons with rapid CAG repeat expansion, suggesting that ASO treatment could be effective even in HD individuals with high polygenic risk from genetic variants that promote somatic expansion.

Understanding the mechanisms of CAG repeat contraction is of therapeutic interest, and our data provide insights into this process. We observed a subtle bias toward CAG contraction in HD iPSC–derived striatal cells lacking MSH3, which is consistent with previous reports of repeat contraction during intergenerational transmission in Msh3-deficient transgenic mice, including DM1, HD, FRDA (Friedrich's ataxia), and FXS mouse models (*26*, *30*, *32*, *74*). The absence of MutSβ in LoVo adenocarcinoma cell extracts increases contraction of a plasmid-based CTG•CAG repeat (*75*). Similarly, Msh2 deficiency increased both intergenerational and somatic contractions in a DM1 mouse model (*76*). In two distinct human cell models harboring CTG repeat expansions of varying length (CTG-22 and CTG-800), contractions were still permitted in MSH3-deficient cells (*34*, *35*). Last, in an hTERT-immortalized retinal pigment epithelial cell model (RPE-1) of CAG repeat instability, MSH3 deficiency resulted in contractions of the repeat over time (*77*). Collectively, the data presented here, alongside these earlier findings, suggest that CAG repeat contraction, but not expansion, can continue in the absence of MutSβ.

Our bulk RNA-seq data revealed ASO chemistry effects and ASO sequence-specific effects on the global transcriptome but a safe *MSH3* lowering profile with no dysregulation of DNA repair pathways. The delivery of ASOs themselves, regardless of target, was positively associated with transcriptomic modules enriched for ribosomal and mitochondrial processes, as well as plasma membrane and structural activity. After controlling for these ASO chemistry effects by comparing with a scrambled ASO, two *MSH3*-targeting ASOs showed no disrupted pathways, whereas one was negatively associated with a module enriched for synaptic membrane and morphogenesis, likely attributable to off-target effects. These 3-10-3 constrained ethyl (cEt)–modified gapmer phosphorothioate ASOs were chosen as tool compounds for their enhanced potency. However, their notable off-target effects related to chemistry and sequence highlight that further optimization would be necessary before their therapeutic use in humans. The disparity in module dysregulation between *MSH3* ASOs is unlikely to be explained by differences in

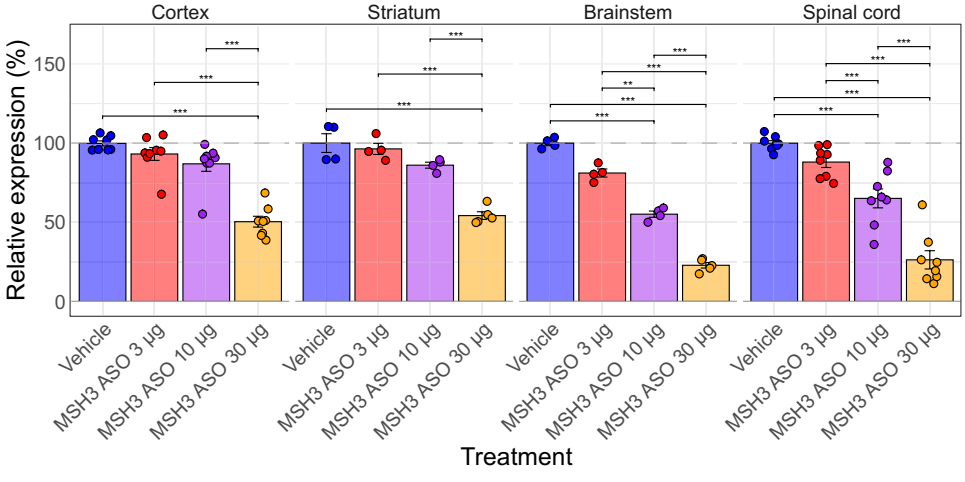

Fig. 6. In vivo target engagement of the *MSH3* ASO in *MSH3* knock-in mice. Human *MSH3* knock-in mice were treated with vehicle (PBS, $n = 8$) or *MSH3* ASO-1 at doses of 3 µg ($n = 8$), 10 µg ($n = 8$), or 30 µg ($n = 8$), delivered via ICV injection. Brain and spinal cord tissues were harvested 14 days after treatment. The graph shows qRT-PCR analysis of *MSH3* expression in mouse brain tissue. Data were analyzed using a two-way ANOVA with post hoc multiple pairwise comparisons using the estimated marginal means R package, with *P* values adjusted for multiple testing using the Benjamini-Hochberg method (data file S8). ***$P < 0.001$ and **$P < 0.01$.

MSH3 lowering, which were not significant, particularly because there is no evidence elsewhere in the literature to suggest that MSH3 has a role in regulating the expression of synaptic genes (*29*). Our snRNA-seq data replicated the effects of *MSH3* ASO-1 treatment, demonstrating down-regulation of pathways involved in synaptic structures and neuronal development. *MSH3* ASO treatment reduced *MSH3* abundance in all cell clusters, suggesting that the ASO was taken up successfully by all cell types within the culture. Moreover, the broader effects of ASO treatment did not appear to be cell-type specific.

We generated a human *MSH3* knock-in mouse model, which represents a valuable tool for testing and developing *MSH3*-targeting therapies. The *MSH3* ASO showed efficient knockdown of *MSH3* in multiple brain regions of the knock-in mice, validating the modulation of human *MSH3* in vivo. We demonstrated 46% ASO-mediated *MSH3* knockdown in the striatum compared with vehicle-treated knock-in animals, which would be expected to substantially reduce somatic CAG repeat expansion on the basis of previous studies (*28*).

This study has several limitations. In HD iPSC–derived striatal neurons, small absolute changes in CAG repeat length were observed over the experimental time frame, likely reflecting the post-mitotic nature of the system. This is consistent with previous reports in similar models (*40*) and mirrors the gradual repeat expansion observed in the human brain over decades. However, this limits the ability to detect subtle effects over short periods, particularly given natural biological variability in iPSC differentiation, such as small differences in starting repeat length and culture composition. In addition, small-pool PCR used to assess rare expansion and contraction events is semiquantitative and limited in statistical power to detect differences between treatment conditions because of the low number of DNA templates per reaction, the rarity of large instability events, and the limited number of reactions that can feasibly be run. These limitations could be addressed in the future with high-throughput approaches, such as single molecule barcoded amplicon sequencing. In addition, 2 weeks of *MSH3* modulation may be insufficient to produce long-term effects on genome dysregulation and should be interpreted cautiously, although RNA-seq analysis of striatal tissue from HD zQ175 mice has shown no effect of MSH3 deficiency even at 6 months of age (*29*). Last, in the *MSH3* knock-in mouse model, dose response or ASO effect duration was not assessed because this study focused on understanding the biology of MSH3 lowering rather than developing a lead therapeutic candidate. Future studies with HD mice could evaluate the impact of *MSH3* knockdown on disease phenotype. However, previous studies showed that whereas MSH3 knockout ablated repeat expansion and corrected histopathology, no phenotypic changes were observed (*26, 28, 29*). This is likely due to the short lifespan of mice and their long inherited CAG repeats already exceeding cellular toxicity thresholds, thereby limiting the potential benefits of preventing further CAG repeat expansion.

Human genetics studies have already validated the therapeutic potential of MSH3 lowering. An *MSH3* polymorphism that causes a subtle ~10% reduction in expression was associated with reduced somatic CAG repeat expansion and slower progression of both clinical and brain imaging measures, as well as a 1.05-year delay in disease onset in patients with HD (*21*). Moreover, heterozygous loss-of-function mutations in *MSH3* led to a 10.6-year delay in HD onset (*40*, *41*). Drug discovery programs that are based on validated human genetics such as this have a greater chance of success (*78*), and here, the human genetics suggest that targeting somatic CAG expansion is key. MSH3 is a prime therapeutic candidate because it is required for repeat expansion and is relatively tolerant of loss of function, particularly in the CNS (*28*, *63*). Human genetics literature shows rare associations of MSH3 deficiency with colorectal adenomas (*56–60*). Targeting MSH3 lowering in the CNS, for example, through an intrathecally delivered ASO, would limit systemic exposure and mitigate colorectal concerns.

Our study finds that ASO-mediated *MSH3* knockdown prevents CAG repeat expansion without significant transcriptional dysregulation associated with *MSH3* reduction in human striatal neuronal cultures, underscoring its potential for the treatment of HD and other repeat expansion disorders in which MSH3 is implicated. The generation of a human *MSH3* knock-in mouse model provides a platform for the development of such treatments. The challenge now lies in translating these therapies into meaningful clinical trials. The new HD integrated staging system (*79*) supports such trials being conducted in the earliest phases of the disease, before clinical manifestation, to allow somatic CAG expansion to be targeted before overt toxicity. However, this will also need to be balanced with selecting a disease stage at which an effect would be measurable over the course of a clinical trial.

MATERIALS AND METHODS

Study design

This study was designed to identify how much MSH3 lowering by an ASO was required to alter somatic instability in human HD iPSC–derived striatal neurons, the most vulnerable cell type in the HD brain. Cultures enriched for HD human iPSC–derived striatal medium spiny neurons were generated from the QS5.1 iPSC cell line derived from a patient with HD with 125 CAG repeats in *HTT* (the 125 CAG iPSC line), using the Arber *et al.* differentiation protocol (*68*). After differentiation, the HD iPSC–derived striatal neuronal cultures were treated continuously from day 36 (referred to as baseline) with *MSH3* ASO or with scrambled (SCR) ASO or vehicle (PBS) as controls. CRISPR-Cas9 was used to edit the 125 CAG iPSC line to generate *MSH3* knockout ($MSH3^{-/-}$) and *FAN1* knockout ($FAN1^{-/-}$) iPSC lines. CAG repeat length was monitored by fragment analysis and small-pool PCR, measuring changes from baseline over time. The effect of *MSH3* ASO on the global transcriptome was assessed using both bulk RNA-seq and snRNA-seq. Last, treatment of a knock-in mouse model expressing the human *MSH3* gene (fig. S12) with *MSH3* ASO–delivered ICV demonstrated ASO target engagement and reduced *MSH3* expression in mouse brain.

ASO sequence and structure

Our study used 3-10-3 cEt gapmer phosphorothioate ASOs, which include the addition of 2′4′-constrained-2′-*O*-ethyl chemical modification, commonly used to increase stability, enhance binding affinity, and, hence, increase potency. *MSH3* ASO-1, selected as our primary *MSH3* targeting ASO owing to its potency, had the sequence GCTTTTGGACCGTTTG and targeted *MSH3* exon 4. *MSH3* ASO-2 (AGAAGATAGCTGGTAG, exon 7) and *MSH3* ASO-3 (GTATATTGATGTAGGT, intron 8) were included as additional *MSH3*-targeting ASOs in our RNA-seq experiment. Our scrambled ASO had the nontargeting sequence

GGCTACTACGCCGTCA, with the same 3-10-3 cEt chemical structure as the *MSH3* ASOs.

Human iPSC line maintenance and differentiation

The QS5.1 125 CAG iPSC line (IRB number: CENSOi019-A) was derived from blood samples drawn from a 7-year-old female pediatric patient with HD after full informed consent from the parent and ethical approval from the local ethics committee with good clinical practice compliance. The iPSC line was generated by Sendai reprogramming at Censo Biotechnologies. It was tested and found to be karyotypically normal even after prolonged culture over 1 year. This iPSC line originally had a repeat sequence containing 125 uninterrupted *HTT* CAG repeats, followed by a single CAACAG cassette, and exhibited CAG repeat expansion in culture. Before differentiation, QS5.1 125 CAG iPSCs were maintained in Essential 8 (E8) Flex medium and were passaged at ~80% confluency using ReLeSR at a 1:6 ratio—typically every 3 to 5 days. Differentiation into medium spiny neuron–enriched striatal cultures was achieved after the 36-day protocol as described in Arber *et al.* (*68*), which involves the promotion of lateral ganglionic eminence fate via activin A treatment, followed by terminal differentiation into striatal neurons. Before terminal differentiation, the cells were passaged onto Geltrex-coated plates to ensure that they remained adherent during long-term culture. Cultures were treated continuously with *MSH3*-targeting ASOs from day 36 of the differentiation process when they are known to express striatal neuronal markers. Neurons were not passaged after this stage, but entire wells were harvested every 3 to 4 weeks to monitor CAG repeat instability.

CRISPR-Cas9 gene editing

Genetic editing of the *MSH3* and *FAN1* genes in the 125 CAG iPSC line was accomplished by electroporation with Cas9 protein and synthetic guide RNA (gRNA) complexes using the P3 Primary Cell 4D Nucleofector X kit L (Lonza, catalog no. V4XP-3024). An hour before nucleofection, iPSCs were changed into E8 Flex medium with 10 μM Rho kinase inhibitor. The gRNA complex was assembled by annealing a target-specific cRNA with an ATTO 550–tagged tracrRNA, which was then incubated with Cas9 protein at room temperature for 20 min. Cells were dissociated with Accutase for 10 min at 37°C, spun down, and resuspended in Lonza P3 solution with the gRNA/Cas9 complex. Cells were transferred to Nucleocuvettes, electroporated using the 4D-Nucleofector (P3 primary cell buffer; program CA137), and then reseeded into six-well plates. After overnight incubation, the cells were detached with Accutase and fluorescence-activated cell–sorted to collect ATTO 550–positive cells. These were seeded sparsely into 10-cm dishes, and colonies were manually picked 3 to 5 days later using an in-hood microscope. The *MSH3* exon 1 or *FAN1* exon 2 loci of successfully isolated clones were Sanger sequenced to identify clones with knockout edits [*MSH3* forward (Fw): CCATGTCTCGCCGGAAG; *MSH3* reverse (Rv): GCCTATCTCCTCAAACGGAAG; *FAN1* Fw: GTCAGAAGGGAAACCTCCTG; *FAN1* Rv: TGTGGACTAGAACCGGCAAA]. The clones were confirmed as *MSH3* or *FAN1* knockout by Western blotting.

qRT-PCR of iPSC-derived neuronal samples

RNA was extracted with the RNeasy Mini Plus (Qiagen) kit, and the SuperScript IV First-Strand Synthesis System (Thermo Fisher Scientific, catalog no. 18091050) was used to transcribe RNA to cDNA, with both steps performed according to the manufacturer's instructions. qRT-PCRs were prepared using 20-ng template in 15-μl reactions with TaqMan Fast Advanced Master Mix (Thermo Fisher Scientific) with exon-spanning TaqMan assays to *MSH3* (*MSH3*: Hs00989003_m1) and run on a QuantStudio5 machine (Thermo Fisher Scientific). The PCR cycling conditions used were as follows: 95°C for 40 s, followed by 40 cycles of 95°C for 15 s and 60°C for 30 s. All reactions were run in triplicate, and three endogenous reference genes (*ATP5B*: Hs00969569_m1, *EIF4A2*: Hs00756996_g1, *UBC*: Hs00824723_m1) were included for normalization purposes. Differences in gene expression were assessed using the ΔΔCt method.

Western blotting of iPSC-derived neuronal samples

Protein was extracted by incubating in radioimmunoprecipitation assay buffer [supplemented with 2× Halt protease inhibitor and benzonase (250 U/ml)] before 4°C centrifugation at 20,000*g* for 15 min. The supernatant was then processed using the NuPage gel electrophoresis system (Invitrogen). Protein was transferred onto polyvinylidene difluoride membrane using the XCell II Blot Module and blocked in fluorescent blocking buffer (Rockland, catalog no. MB-070) for 1 hour. Primary antibodies [mouse α-MSH3 (1:500), BD Biosciences, catalog no. 611390; rabbit α-MSH2 (1:1000), Cell Signaling Technology, catalog no. D24B5; mouse α-MSH6 (1:1000), BD Biosciences, catalog no. 610919; and rabbit α-actin (1:10,000), Abcam, catalog no. ab8227] were prepared in the same buffer and incubated overnight at 4°C. Membranes were washed three times for 10 min in 1% Tween in Dulbecco's PBS (D-PBS) and probed with IRDye-conjugated secondary antibodies at 1:10,000 (donkey α-mouse 680, LI-COR, catalog no. 926-68072; donkey α-rabbit 800, LI-COR, catalog no. 926-32213) for 1 hour at room temperature (RT). Membranes were imaged on the LI-COR Odyssey CLx imaging system and analyzed with Image Studio Lite software.

Immunostaining of iPSC-derived neuronal samples

Cells at days 28 to 30 of the differentiation protocol were seeded on CellCarrier-96 Ultra microplates (PerkinElmer) at a density of 20,000 cells per well. Plates were fixed at the indicated time points using 4% paraformaldehyde. The cells were permeabilized with 0.2% Triton X-100 for 15 min and blocked for 1 hour with D-PBS containing 1% goat serum and 1% bovine serum albumin (BSA). After aspiration, primary antibodies [rabbit α-DARPP32 (1:200), Abcam catalog no. ab40802; mouse α-FOXP1 (1:1000), Abcam, catalog no. ab32010; chicken α-MAP2 (1:1000), Abcam, catalog no. ab5392; rabbit α-Sox2 (1:200), Abcam, catalog no. ab97959; and mouse α-Ki67 (1:500), BD Biosciences, catalog no. 550609] were added in 1% BSA in D-PBS and incubated at 4°C overnight. After D-PBS washes, the cells were incubated with Alexa Fluor–conjugated secondary antibodies at 1:10,000 (goat α-rabbit 488, Thermo Fisher Scientific, catalog no. a11008; goat α-mouse 568, Thermo Fisher Scientific, catalog no. a11031; and goat α-chicken 647, Thermo Fisher Scientific, catalog no. a21449) (RT; 1 hour maximum), washed again before adding Hoechst 33342 (1:10,000, Thermo Fisher Scientific, catalog no. 62249), washed again three times, and then kept in 100 μl of D-PBS with 0.02% sodium azide until being processed on the Opera Phoenix high-content imaging system. Confocal images were analyzed using Columbus software, involving the generation of custom modular scripts to define cellular regions. A "secondary antibody only" control was used to set fluorescence thresholds.

Fragment analysis *HTT* CAG repeat sizing

DNA was extracted with QIAamp DNA Mini kit (Qiagen), and bulk measurement of the *HTT* exon 1 CAG repeat length for each sample was carried out by fragment analysis. In brief, 100 ng of DNA was used for amplification of *HTT* exon 1 by 6-FAM–labeled PCR primers, and the amplicons were resolved by capillary electrophoresis on an ABI 3730xl genetic analyzer (Thermo Fisher Scientific) with the MapMarker 1000 ROX size standard (Eutogentec). Primers used were HTT_exon_1_F:6FAM-CCTTCGAGTCCCTCAAGTCCTT; HTT_exon_1_R:CGGCTGAGGCAGCAGCGGCTGT). PCR conditions were 95°C for 10 min, followed by 30 cycles of 95°C for 30 s, 58°C for 30 s, 72°C for 90 s, and a final cycle of 72°C for 7 min.

The size standard was aligned using GeneMapper (Thermo Fisher Scientific). The mode, median, SD, and instability index of the pathogenic repeat were calculated as previously described using a custom program, available at https://michaelflower.org (*70*, *71*). Instability index (*12*, *80*) was calculated relative to the baseline time point (day 36 of differentiation and day 0 of treatment) for each differentiation and genotype. Quality control removed samples that were poorly amplified (<40 relative fluorescence units) and outlying technical replicates (>1.5 SDs from the mean). The primary instability metric used was instability index relative to control, which is a measure of skewness of the repeat length distribution relative to the mean repeat length of the baseline (control) samples. It was calculated as the sum of the change in repeat length, multiplied by proportional peak area, for each peak in the distribution. To compare CAG instability between groups, the lmer R package was used to generate a linear mixed-effects model analysis of covariance (ANCOVA) with random intercept and random slope for time within differentiation: lmer(instability_metric ~ treatment * time + (1 + time | differentiation)). This model allows for random intercepts for each differentiation and random slopes of instability over time and accounts for the variability in baseline CAG length and its trajectory over time within each differentiation. To explore differences between groups in change of instability index over time, pairwise comparisons were performed using the emtrends function from the emmeans R package, which estimates marginal means for linear trends. These comparisons were adjusted for multiple testing using the Bonferroni method.

Small-pool PCR CAG repeat sizing

As previously described (*10*, *81*, *82*), this involved the serial dilution of genomic DNA into multiple PCRs such that the input for each contained ~500 pg of DNA (i.e., a "small pool"). Limiting the number of input DNA templates reduces PCR competition with the nonexpanded allele. PCR products were then resolved by agarose gel electrophoresis, transferred onto a nylon membrane, and hybridized with a radiolabeled probe specific to CTG•CAG repeats (DM56). Allele repeat lengths were estimated using GelAnalyzer software. Quantifications were carried out by counting the number of rare events outside the range detected by fragment analysis and normalizing to number of lanes. Differences between conditions were assessed by one-way analysis of variance (ANOVA).

Bulk and snRNA-seq

Bulk and snRNA-seq were performed to investigate the transcriptional impact of *MSH3* suppression in HD iPSC–derived striatal neurons. Bulk RNA-seq identified 63,187 transcripts, with stringent quality control filtering resulting in 17,667 genes for analysis. Differential expression analysis was performed using DESeq2, with downstream pathway enrichment conducted using ShinyGO and the GSEABase goSlim function. WGCNA was used to identify gene modules with correlated expression patterns. For snRNA-seq, neuronal nuclei were processed with the 10X Chromium platform, aligned to Genome Reference Consortium Human Build 38 (GRCh38), and normalized for library size. Leiden clustering identified transcriptionally distinct populations, with gene expression changes analyzed across clusters. (Full methods are available in the Supplementary Materials. See also figs. S13 to S15 and table S3).

MSH3 knock-in mice

The human *MSH3* knock-in mouse model used in this study is a constitutive line generated through homologous recombination in collaboration with Taconic Biosciences (fig. S12A). Specifically, mouse genomic sequence from codon K54 in exon 2 to codon G449 in exon 10 from the ENSMUST000000185852 *Msh3* transcript was replaced with its human counterpart ENST00000265081.7 *MSH3* transcript. The positive selection markers, neomycin resistance (NeoR) and puromycin resistance (PuroR), were flanked by flippase recognition target and F3 sites, respectively, and inserted into introns 2 and 9. The targeting vector was generated using bacterial artificial chromosome (BAC) clones from the mouse C57BL/6J PRCI-23 and human PRCI-11 BAC libraries and was transfected into the Taconic Biosciences C57BL/6N Tac ES cell line. Homologous recombinant clones were isolated using double-positive (NeoR and PuroR) and -negative (thymidine kinase) selections. The humanized allele was obtained after flippase-mediated removal of the selection markers. The chimeric mouse-human *MSH3* gene was expressed under the control of endogenous mouse *Msh3* promoter and thus should recapitulate the expression pattern of the mouse *Msh3* gene. *MSH3* knock-in mice of mixed sex at 2 to 3 months of age were used in these experiments. Studies were approved by Ionis Institutional Animal Care and Use Committee (IACUC) protocol 1176. Animals were only included in the study if they were bright, alert, and well kept; animals with cloudy eyes or that were unkempt were excluded.

ICV injection method

Mice were anesthetized with 3% isoflurane gas anesthesia in either air or oxygen carrier gas using an induction box. The animals were placed in a stereotactic apparatus. Anesthesia was maintained with 2% isoflurane by a nose cone fitted to the stereotactic instrument. For each animal, a ~1.0-cm slightly off center (to the right) incision was made in the scalp. The subcutaneous tissue and periosteum were scraped from the skull with a dry sterile cotton tipped applicator. For ICV bolus injections, the coordinates 0.3 mm anterior to bregma, 1.0 mm right lateral, and −3.0 mm ventral were used. Ten microliters of injection solution was injected by hand at injection rates of approximately 1 μl/s with a 3-min wait after completion of injection. The incision was sutured closed using one horizontal mattress stitch with 5-O Ethilon suture. The animals were then allowed to recover from the anesthesia in their home cage. All animals were randomly assigned to each condition, and technicians were blinded to treatment conditions.

qRT-PCR of mouse brain tissue

Each brain region and spinal cord sample was homogenized in 1 ml of TRIzol reagent (Thermo Fisher Scientific), and total RNA was extracted using the Qiagen RNeasy kit (Qiagen) according to the

manufacturer's protocol. After purification, the RNA samples were subjected to real-time qRT-PCR analysis using the Life Technologies ABI QuantStudio 7 Flex Sequence Detection System (Applied Biosystems Inc). Briefly, qRT-PCR reactions were run with the AgPath-ID One-Step qRT-PCR Kit (Thermo Fisher Scientific) reagents and the following primer probe sets: *MSH3* Fw CAAGCCTGCAGCCAGTAG; Rv GCTGTATTCAAAATAAATGTTATCCATCC: *Ppia* Fw TCGCCGCTTGCTGCA; Rv ATCGGCCGTGATGTCGA. Target *MSH3* mRNA was then normalized to *Ppia*, a ubiquitously expressed housekeeping gene, and presented relative to animals treated with vehicle. Differences between conditions were analyzed by two-way ANOVA. Outliers were not removed for analysis, and no animals were excluded from the analysis.

Statistical analyses

All data were analyzed using R (v4.3.1). *MSH3* ASO dose titration curves were fitted using a $y \sim \log(x)$ function. IC_{50} was calculated by two methods: (i) A dose-response model was fitted using the "drm" function from the drc package, and the IC_{50} was extracted using the ED function; (ii) we used linear interpolation, which involved performing a linear regression on log-transformed dose-response data to predict response values over a range of doses. Using the approx function, we interpolated the dose corresponding to a 50% response.

To compare CAG repeat instability rates across groups, we used a linear mixed-effects model [(lmer(instability_metric ~ treatment * time + (1 + time | differentiation)] and performed pairwise comparisons with emtrends, adjusting for multiple testing with Bonferroni (see Fragment Analysis section for more details). The effects of *MSH3* ASO treatment on MSH3 protein amounts in Western blots and CAG repeat instability in small-pool PCR were assessed using one-way ANOVA followed by Bonferroni-corrected post hoc pairwise comparisons. To evaluate the effects of *MSH3* ASO treatment on MSH3 protein across different tissues in the in vivo dose titration experiments, we performed a two-way ANOVA followed by post hoc pairwise comparisons. The two-way ANOVA was conducted using the aov function with the following model: level ~ treatment * tissue. Post hoc pairwise comparisons were performed using the emmeans function, and the resulting *P* values were Bonferroni adjusted for multiple testing.

Supplementary Materials

The PDF file includes:
Materials and Methods
Fig. S1 to S15
Tables S1 to S3
References (*83*–*89*)

Other Supplementary Material for this manuscript includes the following:
Data files S1 to S8
MDAR Reproducibility Checklist

REFERENCES AND NOTES

1. M. E. MacDonald, C. M. Ambrose, M. P. Duyao, R. H. Myers, C. Lin, L. Srinidhi, G. Barnes, S. A. Taylor, M. James, N. Groot, H. MacFarlane, B. Jenkins, M. A. Anderson, N. S. Wexler, J. F. Gusella, G. P. Bates, S. Baxendale, H. Hummerich, S. Kirby, M. North, S. Youngman, R. Mott, G. Zehetner, Z. Sedlacek, A. Poustka, A.-M. Frischauf, H. Lehrach, A. J. Buckler, D. Church, L. Doucette-Stamm, M. C. O'Donovan, L. Riba-Ramirez, M. Shah, V. P. Stanton, S. A. Strobel, K. M. Draths, J. L. Wales, P. Dervan, D. E. Housman, M. Altherr, R. Shiang, L. Thompson, T. Fielder, J. J. Wasmuth, D. Tagle, J. Valdes, L. Elmer, M. Allard, L. Castilla, M. Swaroop, K. Blanchard, F. S. Collins, R. Snell, T. Holloway, K. Gillespie, N. Datson, D. Shaw, P. S. Harper, A novel gene containing a trinucleotide repeat that is expanded and unstable on Huntington's disease chromosomes. *Cell* **72**, 971–983 (1993).
2. N. A. Aziz, M. J. van Belzen, I. D. Coops, R. D. M. Belfroid, R. A. C. Roos, Parent-of-origin differences of mutant HTT CAG repeat instability in Huntington's disease. *Eur. J. Med. Genet.* **54**, e413–e418 (2011).
3. M. Duyao, C. Ambrose, R. Myers, A. Novelletto, F. Persichetti, M. Frontali, S. Folstein, C. Ross, M. Franz, M. Abbott, J. Gray, P. Conneally, A. Young, J. Penney, Z. Hollingsworth, I. Shoulson, A. Lazzarini, A. Falek, W. Koroshetz, D. Sax, E. Bird, J. Vonsattel, E. Bonilla, J. Alvir, J. Bickham Conde, J. H. Cha, L. Dure, F. Gomez, M. Ramos, J. Sanchez-Ramos, S. Snodgrass, M. de Young, N. Wexler, C. Moscowitz, G. Penchaszadeh, H. MacFarlane, M. Anderson, B. Jenkins, J. Srinidhi, G. Barnes, J. Gusella, M. MacDonald, Trinucleotide repeat length instability and age of onset in Huntington's disease. *Nat. Genet.* **4**, 387–392 (1993).
4. M. E. MacDonald, G. Barnes, J. Srinidhi, M. P. Duyao, C. M. Ambrose, R. H. Myers, J. Gray, P. M. Conneally, A. Young, J. Penney, Gametic but not somatic instability of CAG repeat length in Huntington's disease. *J. Med. Genet.* **30**, 982–986 (1993).
5. H. Telenius, B. Kremer, Y. P. Goldberg, J. Theilmann, S. E. Andrew, J. Zeisler, S. Adam, C. Greenberg, E. J. Ives, L. A. Clarke, M. R. Hayden, Somatic and gonadal mosaicism of the Huntington disease gene CAG repeat in brain and sperm. *Nat. Genet.* **6**, 409–414 (1994).
6. V. C. Wheeler, W. Auerbach, J. K. White, J. Srinidhi, A. Auerbach, A. Ryan, M. P. Duyao, V. Vrbanac, M. Weaver, J. F. Gusella, A. L. Joyner, M. E. MacDonald, Length-dependent gametic CAG repeat instability in the Huntington's disease knock-in mouse. *Hum. Mol. Genet.* **8**, 115–122 (1999).
7. V. C. Wheeler, F. Persichetti, S. M. McNeil, J. S. Mysore, S. S. Mysore, M. E. MacDonald, R. H. Myers, J. F. Gusella, N. S. Wexler, US–Venezuela Collaborative Research Group, Factors associated with HD CAG repeat instability in Huntington disease. *J. Med. Genet.* **44**, 695–701 (2007).
8. C. Zühlke, O. Rless, B. Bockel, H. Lange, U. Thies, Mitotic stability and meiotic variability of the (CAG)n repeat in the Huntington disease gene. *Hum. Mol. Genet.* **2**, 2063–2067 (1993).
9. K. E. De Rooij, P. A. M. De Koning Gans, R. A. C. Roos, G.-J. B. Van Ommen, J. T. Den Dunnen, Somatic expansion of the $(CAG)^n$ repeat in Huntington disease brains. *Hum. Genet.* **95**, 270–274 (1995).
10. L. Kennedy, E. Evans, C. M. Chen, L. Craven, P. J. Detloff, M. Ennis, P. F. Shelbourne, Dramatic tissue-specific mutation length increases are an early molecular event in Huntington disease pathogenesis. *Hum. Mol. Genet.* **12**, 3359–3367 (2003).
11. L. Kennedy, P. F. Shelbourne, Dramatic mutation instability in HD mouse striatum: Does polyglutamine load contribute to cell-specific vulnerability in Huntington's disease? *Hum. Mol. Genet.* **9**, 2539–2544 (2000).
12. R. Mouro Pinto, L. Arning, J. V. Giordano, P. Razghandi, M. A. Andrew, T. Gillis, K. Correia, J. S. Mysore, D.-M. Grote Urtubey, C. R. Parwez, S. M. von Hein, H. B. Clark, H. P. Nguyen, E. Förster, A. Beller, S. Jayadaev, C. D. Keene, T. D. Bird, D. Lucente, J.-P. Vonsattel, H. Orr, C. Saft, E. Petrasch-Parwez, V. C. Wheeler, Patterns of CAG repeat instability in the central nervous system and periphery in Huntington's disease and in spinocerebellar ataxia type 1. *Hum. Mol. Genet.* **29**, 2551–2567 (2020).
13. P. F. Shelbourne, C. Keller-McGandy, W. L. Bi, S.-R. Yoon, L. Dubeau, N. J. Veitch, J. P. Vonsattel, N. S. Wexler, The US-Venezuela Collaborative Research Group, N. Arnheim, S. J. Augood, Triplet repeat mutation length gains correlate with cell-type specific vulnerability in Huntington disease brain. *Hum. Mol. Genet.* **16**, 1133–1142 (2007).
14. M. Swami, A. E. Hendricks, T. Gillis, T. Massood, J. Mysore, R. H. Myers, V. C. Wheeler, Somatic expansion of the Huntington's disease CAG repeat in the brain is associated with an earlier age of disease onset. *Hum. Mol. Genet.* **18**, 3039–3047 (2009).
15. M. Ciosi, A. Maxwell, S. A. Cumming, D. J. Hensman Moss, A. M. Alshammari, M. D. Flower, A. Durr, B. R. Leavitt, R. A. C. Roos, P. Holmans, L. Jones, D. R. Langbehn, S. Kwak, S. J. Tabrizi, D. G. Monckton, A genetic association study of glutamine-encoding DNA sequence structures, somatic CAG expansion, and DNA repair gene variants, with Huntington disease clinical outcomes. *EBioMedicine* **48**, 568–580 (2019).
16. N. J. Veitch, M. Ennis, J. P. McAbney, US-Venezuela Collaborative Research Project, P. F. Shelbourne, D. G. Monckton, Inherited CAG.CTG allele length is a major modifier of somatic mutation length variability in Huntington disease. *DNA Repair* **6**, 789–796 (2007).
17. Genetic Modifiers of Huntington's Disease (GeM-HD) Consortium, CAG repeat not polyglutamine length determines timing of Huntington's disease onset. *Cell* **178**, 887–900.e14 (2019).
18. G. E. B. Wright, J. A. Collins, C. Kay, C. McDonald, E. Dolzhenko, Q. Xia, K. Bečanović, B. I. Drögemöller, A. Semaka, C. M. Nguyen, B. Trost, F. Richards, E. K. Bijlsma, F. Squitieri, C. J. D. Ross, S. W. Scherer, M. A. Eberle, R. K. C. Yuen, M. R. Hayden, Length of uninterrupted CAG, independent of polyglutamine size, results in increased somatic instability, hastening onset of Huntington disease. *Am. J. Hum. Genet.* **104**, 1116–1126 (2019).
19. Genetic Modifiers of Huntington's Disease (GeM-HD) Consortium, Identification of genetic factors that modify clinical onset of Huntington's disease. *Cell* **162**, 516–526 (2015).

20. E. P. Hong, M. E. MacDonald, V. C. Wheeler, L. Jones, P. Holmans, M. Orth, D. G. Monckton, J. D. Long, S. Kwak, J. F. Gusella, J.-M. Lee, Huntington's disease pathogenesis: Two sequential components. *J. Huntingtons Dis.* **10**, 35–51 (2021).
21. D. J. H. Moss, A. F. Pardinas, D. Langbehn, K. Lo, B. R. Leavitt, R. Roos, A. Durr, S. Mead, P. Holmans, L. Jones, S. J. Tabrizi, Identification of genetic variants associated with Huntington's disease progression: A genome-wide association study. *Lancet Neurol.* **16**, 701–711 (2017).
22. J.-M. Lee, Y. Huang, M. Orth, T. Gillis, J. Siciliano, E. Hong, J. S. Mysore, D. Lucente, V. C. Wheeler, I. S. Seong, Z. L. McLean, J. A. Mills, B. McAllister, S. V. Lobanov, T. H. Massey, M. Ciosi, G. B. Landwehrmeyer, J. S. Paulsen, E. R. Dorsey, I. Shoulson, C. Sampaio, D. G. Monckton, S. Kwak, P. Holmans, L. Jones, M. E. MacDonald, J. D. Long, J. F. Gusella, Genetic modifiers of Huntington disease differentially influence motor and cognitive domains. *Am. J. Hum. Genet.* **109**, 885–899 (2022).
23. R. R. Iyer, A. Pluciennik, V. Burdett, P. L. Modrich, DNA mismatch repair: Functions and mechanisms. *Chem. Rev.* **106**, 302–323 (2006).
24. F. Palombo, I. Iaccarino, E. Nakajima, M. Ikejima, T. Shimada, J. Jiricny, hMutSβ, a heterodimer of hMSH2 and hMSH3, binds to insertion/deletion loops in DNA. *Curr. Biol.* **6**, 1181–1184 (1996).
25. J. Genschel, S. J. Littman, J. T. Drummond, P. Modrich, Isolation of MutSβ from human cells and comparison of the mismatch repair specificities of MutSβ and MutSα. *J. Biol. Chem.* **273**, 19895–19901 (1998).
26. E. Dragileva, A. Hendricks, A. Teed, T. Gillis, E. T. Lopez, E. C. Friedberg, R. Kucherlapati, W. Edelmann, K. L. Lunetta, M. E. MacDonald, V. C. Wheeler, Intergenerational and striatal CAG repeat instability in Huntington's disease knock-in mice involve different DNA repair genes. *Neurobiol. Dis.* **33**, 37–47 (2009).
27. S. Tomé, K. Manley, J. P. Simard, G. W. Clark, M. M. Slean, M. Swami, P. F. Shelbourne, E. R. M. Tillier, D. G. Monckton, A. Messer, C. E. Pearson, MSH3 polymorphisms and protein levels affect CAG repeat instability in Huntington's disease mice. *PLOS Genet.* **9**, e1003280 (2013).
28. D. O'Reilly, J. Belgrad, C. Ferguson, A. Summers, E. Sapp, C. McHugh, E. Mathews, A. Boudi, J. Buchwald, S. Ly, D. Moreno, R. Furgal, E. Luu, Z. Kennedy, V. Hariharan, K. Monopoli, X. W. Yang, J. Carroll, M. DiFiglia, N. Aronin, A. Khvorova, Di-valent siRNA-mediated silencing of MSH3 blocks somatic repeat expansion in mouse models of Huntington's disease. *Mol. Ther.* **31**, 1661–1674 (2023).
29. S. G. Aldous, E. J. Smith, C. Landles, G. F. Osborne, M. Cañibano-Pico, I. M. Nita, J. Phillips, Y. Zhang, B. Jin, M. B. Hirst, C. L. Benn, B. C. Bond, W. Edelmann, J. R. Greene, G. P. Bates, A CAG repeat threshold for therapeutics targeting somatic instability in Huntington's disease. *Brain* **147**, 1784–1798 (2024).
30. L. Foiry, L. Dong, C. Savouret, L. Hubert, H. te Riele, C. Junien, G. Gourdon, Msh3 is a limiting factor in the formation of intergenerational CTG expansions in DM1 transgenic mice. *Hum. Genet.* **119**, 520–526 (2006).
31. W. van den Broek, M. R. Nelen, D. G. Wansink, M. M. Coerwinkel, H. T. Riele, P. Groenen, B. Wieringa, Somatic expansion behaviour of the $(CTG)_n$ repeat in myotonic dystrophy knock-in mice is differentially affected by Msh3 and Msh6 mismatch-repair proteins. *Hum. Mol. Genet.* **11**, 191–198 (2002).
32. X. N. Zhao, D. Kumari, S. Gupta, D. Wu, M. Evanitsky, W. Yang, K. Usdin, Mutsβ generates both expansions and contractions in a mouse model of the Fragile X-associated disorders. *Hum. Mol. Genet.* **24**, 7087–7096 (2015).
33. A.-M. M. Gannon, A. Frizzell, E. Healy, R. S. Lahue, MutSβ and histone deacetylase complexes promote expansions of trinucleotide repeats in human cells. *Nucleic Acids Res.* **40**, 10324–10333 (2012).
34. R. Nakatani, M. Nakamori, H. Fujimura, H. Mochizuki, M. P. Takahashi, Large expansion of CTG•CAG repeats is exacerbated by MutSβ in human cells. *Sci. Rep.* **5**, (2015).
35. N. Keogh, K. Y. Chan, G.-M. Li, R. S. Lahue, MutSβ abundance and Msh3 ATP hydrolysis activity are important drivers of CTG•CAG repeat expansions. *Nucleic Acids Res.* **45**, 10068–10078 (2017).
36. A. Halabi, S. Ditch, J. Wang, E. Grabczyk, DNA mismatch repair complex MutSβ promotes GAA·TTC repeat expansion in human cells. *J. Biol. Chem.* **287**, 29958–29967 (2012).
37. F. Morales, M. Vásquez, C. Santamaría, P. Cuenca, E. Corrales, D. G. Monckton, A polymorphism in the MSH3 mismatch repair gene is associated with the levels of somatic instability of the expanded CTG repeat in the blood DNA of myotonic dystrophy type 1 patients. *DNA Repair* **40**, 57–66 (2016).
38. M. Flower, V. Lomeikaite, M. Ciosi, S. Cumming, F. Morales, K. Lo, D. H. Moss, L. Jones, P. Holmans, TRACK-HD Investigators, OPTIMISTIC Consortium, D. G. Monckton, S. J. Tabrizi, MSH3 modifies somatic instability and disease severity in Huntington's and myotonic dystrophy type 1. *Brain* **142**, 1876–1886 (2019).
39. B.-H. Laabs, C. Klein, J. Pozojevic, A. Domingo, N. Brüggemann, K. Grütz, R. L. Rosales, R. D. Jamora, G. Saranza, C. C. E. Diesta, M. Wittig, S. Schaake, M. Dulovic-Mahlow, J. Quismundo, P. Otto, P. Acuna, C. Go, N. Sharma, T. Multhaupt-Buell, U. Müller, H. Hanssen, F. Kilpert, A. Franke, A. Rolfs, P. Bauer, V. Dobričić, K. Lohmann, L. J. Ozelius, F. J. Kaiser, I. R. König, A. Westenberger, Identifying genetic modifiers of age-associated penetrance in X-linked dystonia-parkinsonism. *Nat. Commun.* **12**, 3216 (2021).
40. B. McAllister, J. Donaldson, C. S. Binda, S. Powell, U. Chughtai, G. Edwards, J. Stone, S. Lobanov, L. Elliston, L. N. Schuhmacher, E. Rees, G. Menzies, M. Ciosi, A. Maxwell, M. J. Chao, E. P. Hong, D. Lucente, V. Wheeler, J. M. Lee, M. E. MacDonald, J. D. Long, E. H. Aylward, G. B. Landwehrmeyer, A. E. Rosser, J. S. Paulsen, N. M. Williams, J. F. Gusella, D. G. Monckton, N. D. Allen, P. Holmans, L. Jones, T. H. Massey, Exome sequencing of individuals with Huntington's disease implicates FAN1 nuclease activity in slowing CAG expansion and disease onset. *Nat. Neurosci.* **25**, 446–457 (2022).
41. Huntington's Disease Exome and MiSeq Data Access Committee, Whole exome and MiSeq HTT sequencing of Huntington's disease patient samples, European Genome-Phenome Archive, DAC: EGAC00001002778 (2022); https://ega-archive.org/datasets/EGAD00001009077.
42. M. Lek, K. J. Karczewski, E. V. Minikel, K. E. Samocha, E. Banks, T. Fennell, A. H. O'Donnell-Luria, J. S. Ware, A. J. Hill, B. B. Cummings, T. Tukiainen, D. P. Birnbaum, J. A. Kosmicki, L. E. Duncan, K. Estrada, F. Zhao, J. Zou, E. Pierce-Hoffman, J. Berghout, D. N. Cooper, N. Deflaux, M. DePristo, R. Do, J. Flannick, M. Fromer, L. Gauthier, J. Goldstein, N. Gupta, D. Howrigan, A. Kiezun, M. I. Kurki, A. L. Moonshine, P. Natarajan, L. Orozco, G. M. Peloso, R. Poplin, M. A. Rivas, V. Ruano-Rubio, S. A. Rose, D. M. Ruderfer, K. Shakir, P. D. Stenson, C. Stevens, B. P. Thomas, G. Tiao, M. T. Tusie-Luna, B. Weisburd, H.-H. Won, D. Yu, D. M. Altshuler, D. Ardissino, M. Boehnke, J. Danesh, S. Donnelly, R. Elosua, J. C. Florez, S. B. Gabriel, G. Getz, S. J. Glatt, C. M. Hultman, S. Kathiresan, M. Laakso, S. McCarroll, M. I. McCarthy, D. McGovern, R. McPherson, B. M. Neale, A. Palotie, S. M. Purcell, D. Saleheen, J. M. Scharf, P. Sklar, P. F. Sullivan, J. Tuomilehto, M. T. Tsuang, H. C. Watkins, J. G. Wilson, M. J. Daly, D. G. MacArthur, Exome Aggregation Consortium, Analysis of protein-coding genetic variation in 60,706 humans. *Nature* **536**, 285–291 (2016).
43. K. J. Karczewski, B. Weisburd, B. Thomas, M. Solomonson, D. M. Ruderfer, D. Kavanagh, T. Hamamsy, M. Lek, K. E. Samocha, B. B. Cummings, D. Birnbaum, The Exome Aggregation Consortium, M. J. Daly, D. G. MacArthur, The ExAC browser: Displaying reference data information from over 60 000 exomes. *Nucleic Acids Res.* **45**, D840–D845 (2017).
44. R. R. Iyer, A. Pluciennik, DNA mismatch repair and its role in Huntington's disease. *J. Huntingtons Dis.* **10**, 75–94 (2021).
45. N. de Wind, M. Dekker, N. Claij, L. Jansen, Y. van Klink, M. Radman, G. Riggins, M. van der Valk, K. 't van Wout, H. te Riele, HNPCC-like cancer predisposition in mice through simultaneous loss of Msh3 and Msh6 mismatch-repair protein functions. *Nat. Genet.* **23**, 359–362 (1999).
46. W. Edelmann, A. Umar, K. Yang, J. Heyer, M. Kucherlapati, M. Lia, B. Kneitz, E. Avdievich, K. Fan, E. Wong, G. Crouse, T. Kunkel, M. Lipkin, R. D. Kolodner, R. Kucherlapati, The DNA mismatch repair genes Msh3 and Msh6 cooperate in intestinal tumor suppression. *Cancer Res.* **60**, 803–807 (2000).
47. P. Peltomäki, Update on Lynch syndrome genomics. *Fam. Cancer* **15**, 385–393 (2016).
48. P. Peltomäki, Role of DNA mismatch repair defects in the pathogenesis of human cancer. *J. Clin. Oncol.* **21**, 1174–1179 (2003).
49. M. Abedalthagafi, Constitutional mismatch repair-deficiency: Current problems and emerging therapeutic strategies. *Oncotarget* **9**, 35458–35469 (2018).
50. R. A. Barnetson, A. Tenesa, S. M. Farrington, I. D. Nicholl, R. Cetnarskyj, M. E. Porteous, H. Campbell, M. G. Dunlop, Identification and survival of carriers of mutations in DNA mismatch-repair genes in colon cancer. *N. Engl. J. Med.* **354**, 2751–2763 (2006).
51. R. S. Hamad, M. E. Ibrahim, CMMRD caused by PMS1 mutation in a sudanese consanguineous family. *Hered. Cancer Clin. Pract.* **20**, 16 (2022).
52. H. Hampel, W. L. Frankel, E. Martin, M. Arnold, K. Khanduja, P. Kuebler, H. Nakagawa, K. Sotamaa, T. W. Prior, J. Westman, J. Panescu, D. Fix, J. Lockman, I. Comeras, A. de la Chapelle, Screening for the Lynch syndrome (hereditary nonpolyposis colorectal cancer). *N. Engl. J. Med.* **352**, 1851–1860 (2005).
53. G. E. Palomaki, M. R. McClain, S. Melillo, H. L. Hampel, S. N. Thibodeau, EGAPP supplementary evidence review: DNA testing strategies aimed at reducing morbidity and mortality from Lynch syndrome. *Genet. Med.* **11**, 42–65 (2009).
54. R. H. Sijmons, R. M. W. Hofstra, Review: Clinical aspects of hereditary DNA mismatch repair gene mutations. *DNA Repair* **38**, 155–162 (2016).
55. K. Wimmer, J. Etzler, Constitutional mismatch repair-deficiency syndrome: Have we so far seen only the tip of an iceberg? *Hum. Genet.* **124**, 105–122 (2008).
56. R. Adam, I. Spier, B. Zhao, M. Kloth, J. Marquez, I. Hinrichsen, J. Kirfel, A. Tafazzoli, S. Horpaopan, S. Uhlhaas, D. Stienen, N. Friedrichs, J. Altmüller, A. Laner, S. Holzapfel, S. Peters, K. Kayser, H. Thiele, E. Holinski-Feder, G. Marra, G. Kristiansen, M. M. Nöthen, R. Büttner, G. Möslein, R. C. Betz, A. Brieger, R. P. Lifton, S. Aretz, Exome sequencing identifies biallelic MSH3 germline mutations as a recessive subtype of colorectal adenomatous polyposis. *Am. J. Hum. Genet.* **99**, 337–351 (2016).
57. A. S. Aelvoet, D. R. Hoekman, B. J. W. Redeker, J. Weegenaar, E. Dekker, C. J. M. van Noesel, F. A. M. Duijkers, A large family with MSH3-related polyposis. *Fam. Cancer* **22**, 49–54 (2023).
58. M.-C. Villy, J. Masliah-Planchon, A. Schnitzler, H. Delhomelle, B. Buecher, M. Filser, K. Merchadou, L. Golmard, S. Melaabi, S. Vacher, M. Blanluet, V. Suybeng, C. Corsini, M. Dhooge, N. Hamzaoui, S. Farelly, A. Ait Omar, R. Benamouzig, V. Caumette, M. Bahuau,

J. Cucherousset, Y. Allory, D. Stoppa-Lyonnet, I. Bieche, C. Colas, *MSH3*: A confirmed predisposing gene for adenomatous polyposis. *J. Med. Genet.* **60**, 1198–1205 (2023).
59. A. Gavric, M. Krajc, L. Strnisa, A. U. Gavric, S. Plut, *MSH3*-related adenomatous polyposis in a patient with the negative family history of colorectal polyps. *Gastroenterol. Hepatol.* **47**, 397–400 (2024).
60. M. Koi, B. H. Leach, S. McGee, S. S. Tseng-Rogenski, C. A. Burke, J. M. Carethers, Compound heterozygous MSH3 germline variants and associated tumor somatic DNA mismatch repair dysfunction. *NPJ Precis. Oncol.* **8**, 12 (2024).
61. N. Pecina-Slaus, A. Kafka, I. Salamon, A. Bukovac, Mismatch repair pathway, genome stability and cancer. *Front. Mol. Biosci.* **7**, 122 (2020).
62. G. X. Reyes, T. T. Schmidt, R. D. Kolodner, H. Hombauer, New insights into the mechanism of DNA mismatch repair. *Chromosoma* **124**, 443–462 (2015).
63. M. Zhao, Y. Liu, G. Ding, D. Qu, H. Qu, Online database for brain cancer-implicated genes: Exploring the subtype-specific mechanisms of brain cancer. *BMC Genomics* **22**, 458 (2021).
64. C. F. Bennett, B. F. Baker, N. Pham, E. Swayze, R. S. Geary, Pharmacology of antisense drugs. *Annu. Rev. Pharmacol. Toxicol.* **57**, 81–105 (2017).
65. S. T. Crooke, J. L. Witztum, C. F. Bennett, B. F. Baker, RNA-targeted therapeutics. *Cell Metab.* **27**, 714–739 (2018).
66. C. F. Bennett, H. B. Kordasiewicz, D. W. Cleveland, Antisense drugs make sense for neurological diseases. *Annu. Rev. Pharmacol. Toxicol.* **61**, 831–852 (2021).
67. M. E. McCauley, C. F. Bennett, Antisense drugs for rare and ultra-rare genetic neurological diseases. *Neuron* **111**, 2465–2468 (2023).
68. C. Arber, S. V. Precious, S. Cambray, J. R. Risner-Janiczek, C. Kelly, Z. Noakes, M. Fjodorova, A. Heuer, M. A. Ungless, T. A. Rodriguez, A. E. Rosser, S. B. Dunnett, M. Li, Activin A directs striatal projection neuron differentiation of human pluripotent stem cells. *Development* **142**, 1375–1386 (2015).
69. R. Ferguson, R. Goold, L. Coupland, M. Flower, S. J. Tabrizi, Therapeutic validation of MMR-associated genetic modifiers in a human ex vivo model of Huntington disease. *Am. J. Hum. Genet.* **111**, 1165–1183 (2024).
70. R. Goold, M. Flower, D. H. Moss, C. Medway, A. Wood-Kaczmar, R. Andre, P. Farshim, G. P. Bates, P. Holmans, L. Jones, S. J. Tabrizi, FAN1 modifies Huntington's disease progression by stabilizing the expanded HTT CAG repeat. *Hum. Mol. Genet.* **28**, 650–661 (2018).
71. R. Goold, J. Hamilton, T. Menneteau, M. Flower, E. L. Bunting, S. G. Aldous, A. Porro, J. R. Vicente, N. D. Allen, H. Wilkinson, G. P. Bates, A. A. Sartori, K. Thalassinos, G. Balmus, S. J. Tabrizi, FAN1 controls mismatch repair complex assembly via MLH1 retention to stabilize CAG repeat expansion in Huntington's disease. *Cell Rep.* **36**, 109649 (2021).
72. F. Rigo, S. J. Chun, D. A. Norris, H. Gene, L. Sam, M. John, A. F. Robert, G. Hans, H. Yimin, S. G. John, R. K. Adrian, P. H. Scott, C. F. Bennett, Pharmacology of a central nervous system delivered 2′-*O*-methoxyethyl–modified survival of motor neuron splicing oligonucleotide in mice and nonhuman primates. *J. Pharmacol. Exp. Ther.* **350**, 46–55 (2014).
73. R. Driscoll, L. Hampton, N. A. Abraham, J. D. Larigan, N. F. Joseph, J. C. Hernandez-Vega, S. Geisler, F.-C. Yang, M. Deninger, D. T. Tran, N. Khatri, B. M. D. C. Godinho, G. A. Kinberger, D. R. Montagna, W. D. Hirst, C. L. Guardado, K. E. Glajch, H. M. Arnold, C. L. Gallant-Behm, A. Weihofen, Dose-dependent reduction of somatic expansions but not Htt aggregates by di-valent siRNA-mediated silencing of MSH3 in HdhQ111 mice. *Sci. Rep.* **14**, 2061 (2024).
74. V. Ezzatizadeh, R. M. Pinto, C. Sandi, M. Sandi, S. Al-Mahdawi, H. Te Riele, M. A. Pook, The mismatch repair system protects against intergenerational GAA repeat instability in a Friedreich ataxia mouse model. *Neurobiol. Dis.* **46**, 165–171 (2012).
75. M. M. Slean, G. B. Panigrahi, A. L. Castel, A. B. Pearson, A. E. Tomkinson, C. E. Pearson, Absence of MutSβ leads to the formation of slipped-DNA for CTG/CAG contractions at primate replication forks. *DNA Repair* **42**, 107–118 (2016).
76. C. Savouret, E. Brisson, J. Essers, R. Kanaar, A. Pastink, H. te Riele, C. Junien, G. Gourdon, CTG repeat instability and size variation timing in DNA repair-deficient mice. *EMBO J.* **22**, 2264–2273 (2003).
77. Z. L. McLean, G. Dadi, C. Kevin, C. L. R. Jennie, S. Shota, N. F. Iris, V.-M. Zoe, R. Manasa, M. Elisabetta, R. Jayla, G. Tammy, L. Diane, P. K. Benjamin, L. Jong-Min, E. M. Marcy, C. W. Vanessa, P. Ricardo Mouro, F. G. James, *PMS1* as a target for splice modulation to prevent somatic CAG repeat expansion in Huntington's disease. bioRxiv, 2023.2007.2025.550489 [Preprint] (2023).
78. R. M. Plenge, E. M. Scolnick, D. Altshuler, Validating therapeutic targets through human genetics. *Nat. Rev. Drug Discov.* **12**, 581–594 (2013).
79. S. J. Tabrizi, S. Schobel, E. C. Gantman, A. Mansbach, B. Borowsky, P. Konstantinova, T. A. Mestre, J. Panagoulias, C. A. Ross, M. Zauderer, A. P. Mullin, K. Romero, S. Sivakumaran, E. C. Turner, J. D. Long, C. Sampaio, Huntington's Disease Regulatory Science Consortium (HD-RSC), A biological classification of Huntington's disease: The integrated staging system. *Lancet Neurol.* **21**, 632–644 (2022).
80. J.-M. Lee, J. Zhang, A. I. Su, J. R. Walker, T. Wiltshire, K. Kang, E. Dragileva, T. Gillis, E. T. Lopez, M.-J. Boily, M. Cyr, I. Kohane, J. F. Gusella, M. E. MacDonald, V. C. Wheeler, A novel approach to investigate tissue-specific trinucleotide repeat instability. *BMC Syst. Biol.* **4**, 29 (2010).
81. M. Gomes-Pereira, S. I. Bidichandani, D. G. Monckton, "Analysis of unstable triplet repeats using small-pool polymerase chain reaction" in *Trinucleotide Repeat Protocols*, Y. Kohwi, Ed. (Humana Press, 2004), pp. 61–76.
82. D. G. Monckton, L.-J. C. Wong, T. Ashizawa, C. T. Caskey, Somatic mosaicism, germline expansions, germline reversions and intergenerational reductions in myotonic dystrophy males: Small pool PCR analyses. *Hum. Mol. Genet.* **4**, 1–8 (1995).
83. R. Bourgon, R. Gentleman, W. Huber, Independent filtering increases detection power for high-throughput experiments. *Proc. Natl. Acad. Sci. U.S.A.* **107**, 9546–9551 (2010).
84. P. Langfelder, S. Horvath, WGCNA: An R package for weighted correlation network analysis. *BMC Bioinformatics* **9**, 559 (2008).
85. M. I. Love, W. Huber, S. Anders, Moderated estimation of fold change and dispersion for RNA-seq data with DESeq2. *Genome Biol.* **15**, 550 (2014).
86. S. X. Ge, D. Jung, R. Yao, ShinyGO: A graphical gene-set enrichment tool for animals and plants. *Bioinformatics* **36**, 2628–2629 (2020).
87. B. Zhang, S. Horvath, A general framework for weighted gene co-expression network analysis. *Stat. Appl. Genet. Mol. Biol.* **4**, 17 (2005).
88. T. Wu, E. Hu, S. Xu, M. Chen, P. Guo, Z. Dai, T. Feng, L. Zhou, W. Tang, L. Zhan, X. Fu, S. Liu, X. Bo, G. Yu, clusterProfiler 4.0: A universal enrichment tool for interpreting omics data. *Innovation* **2**, 100141 (2021).
89. E. Z. Macosko, A. Basu, R. Satija, J. Nemesh, K. Shekhar, M. Goldman, I. Tirosh, A. R. Bialas, N. Kamitaki, E. M. Martersteck, J. J. Trombetta, D. A. Weitz, J. R. Sanes, A. K. Shalek, A. Regev, S. A. McCarroll, Highly parallel genome-wide expression profiling of individual cells using nanoliter droplets. *Cell* **161**, 1202–1214 (2015).

Acknowledgments: We thank T. Vogt, B. Prasad, and M. Finley for helpful discussions and R. Newton for assistance with figures and tables. We thank Taconic Biosciences for help with generating the *MSH3* knock-in mice and P. Holmans for consultation on statistics. We thank B. McAllister for calculations based on published data (*40*, *41*) regarding the delay in age of disease onset in patients with HD, heterozygous for *MSH3* loss-of-function mutations. **Funding:** This study was supported by the Medical Research Council (MRC) grant #MR/N013867/1 (to E.L.B.); CHDI Foundation (to E.L.B., J.D., M.F., J.O., S.J.T., D.G.M., and S.A.C.); UK Dementia Research Institute (DRI) that receives funding from DRI Ltd., funded by the UK MRC and the CHDI Foundation (to M.F., J.O., S.J.T., and G.B.); and the Romanian Ministry of Research, Innovation, and Digitization grant #PNRR-III-C9-2022-I8-66, contract 760114 (to G.B. and M.M.). This research was funded in whole, or in part, by the Wellcome Trust 223082/Z/21/Z (S.J.T). For the purpose of Open Access, the author has applied a CC BY public copyright license to any author-accepted manuscript version arising from this submission. **Author contributions:** S.J.T. conceived the project. E.L.B. and S.J.T. acquired the funding. S.J.T., D.G.M., J.D., S.A.C., M.F., and G.B. supervised the project. E.L.B. performed immunostaining, Western blotting, and qRT-PCR to characterize HD iPSC–derived neurons and to assess *MSH3* lowering after ASO treatment. E.L.B. performed fragment analysis on long-term iPSC-derived striatal neurons, and M.F. performed statistical analysis. E.L.B. generated and characterized 125 CAG *MSH3* knockout iPSC lines. J.H. generated 125 CAG *FAN1* knockout iPSC lines. S.A.C. and E.L.B. performed SP-PCR experiments, under the supervision of D.G.M. E.L.B., J.D., J.O., and E.B. performed tissue culture for RNA-seq experiments. M.M., M.F., and J.B. performed all data analysis of bulk RNA-seq experiments with input and supervision from G.B. M.T., R.E.H., and W.-S.L. performed snRNA-seq experiments under the supervision of S.A.M. S.L. and B.F. performed all in vivo mouse experiments, under the supervision of H.T.Z. and H.B.K. J.D., M.F., E.L.B., J.H., H.T.Z., J.O., S.A.C., M.M., M.T., G.B., D.G.M., and S.J.T. were involved in visualization and figure production. E.L.B. wrote the original manuscript draft; J.D., E.L.B., M.F., J.O., E.B., H.T.Z., S.A.C., M.M., W.-S.L., M.T., J.B., J.H., B.H., M.R., G.B., S.A.M., F.B., H.B.K., D.G.M., and S.J.T. were involved in writing, reviewing, and editing the manuscript. All authors read and approved the final manuscript. **Competing interests:** S.J.T. has undertaken paid consultancy services for F. Hoffmann–La Roche through UCL Consultants Ltd., a wholly owned subsidiary of University College London (UCL). UCL London Hospitals NHS Foundation Trust, S.J.T.'s host clinical institution, received funding to run clinical trials for F. Hoffman–La Roche. D.G.M. has consulted for or received honoraria/grants from AMO Pharma, Dyne, F. Hoffman–La Roche, LoQus23 Therapeutics, MOMA Therapeutics, Novartis, Ono Pharmaceuticals, Pfizer Pharmaceuticals, Rgenta Therapeutics, Sanofi, Sarepta Therapeutics Inc., Script Biosciences, Triplet Therapeutics, and Vertex Pharmaceuticals. D.G.M. also has research contracts with AMO Pharma and Vertex Pharmaceuticals. S.A.M. has received compensation for scientific advice from F. Hoffman–La Roche, Pfizer Pharmaceuticals, Biogen, Vertex Pharmaceuticals, and LoQus23 Therapeutics. G.B. is the founder and chief executive officer (part time) of Function RX Ltd. E.L.B. is now a full-time employee of F. Hoffman–La Roche. The authors declare that they have no other competing interests. **Data and materials availability:** All data associated with this study are present in the paper or the Supplementary Materials. RNA sequencing data are deposited at SRA: bulk RNA-seq data accession number PRJNA1177884;

snRNA-seq data accession number PRJNA1180543. Individual-level data and statistical analyses are provided in data files S1 to S8. Data and analysis scripts for repeat sizing are available on Zenodo at DOI: 10.5281/zenodo.14670902 and for other analyses at DOI: 10.5281/zenodo.14670875. The original QS5.1 HD 125 CAG iPSC parental line and the gene-edited iPSC lines can be made available to academic researchers under a Materials Transfer Agreement (MTA) upon request to S.J.T. at UCL. Approval by Axol Biosciences may be required for the iPSC parent line. The iPSC parent line can also be made available from Axol Biosciences under a license. The human *MSH3* knock-in mice can be made available under an MTA upon request to H.T.Z. at Ionis.

Submitted 11 December 2023
Accepted 23 January 2025
Published 12 February 2025
10.1126/scitranslmed.adn4600